C. ELEGANS PEZO-1 IS A MECHANOSENSITIVE CHANNEL INVOLVED IN FOOD SENSATION

Jonathan RM Millet[1,2], Luis O Romero[1,3], Jungsoo Lee[1], and Valeria Vásquez[1,*].

[1]Department of Physiology, College of Medicine, University of Tennessee Health Science Center, Memphis, TN 38163, USA

[2] Present address: Institute of Neuroscience, Department of Biology, University of Oregon, Eugene, OR 97403-1254, USA

[3] Integrated Biomedical Sciences Graduate Program, College of Graduate Health Sciences, University of Tennessee Health Science Center, Memphis, TN 38163, USA

*Corresponding Author

Valeria Vásquez (VV)

Email: vvasquez@uthsc.edu

ABSTRACT

PIEZO channels are force sensors essential for physiological processes including baroreception and proprioception. The *Caenorhabditis elegans* genome encodes an ortholog gene of the Piezo family, *pezo-1*, expressed in several tissues including the pharynx. This myogenic pump is an essential component of the *C. elegans* alimentary canal whose contraction and relaxation are modulated by mechanical stimulation elicited by food content. Whether *pezo-1* encodes a mechanosensitive channel and contributes to pharyngeal function remains unknown. Here, we leverage genome editing, genetics, microfluidics, and electropharyngeogram recordings to establish that *pezo-1* is expressed in the pharynx, including a proprioceptive-like neuron, and regulates pharyngeal function. Knockout (KO) and gain-of-function (GOF) mutants reveal that *pezo-1* is involved in fine-tuning pharyngeal pumping frequency, sensing osmolarity and food quality. Using pressure-clamp experiments in primary *C. elegans* embryo cultures, we determine that *pezo-1* KO cells do not display mechanosensitive currents, whereas cells expressing wild-type or GOF PEZO-1 exhibit mechanosensitivity. Moreover, infecting the *Spodoptera frugiperda* cell line with a baculovirus containing the *pezo-1* isoform G (among the longest isoforms) demonstrates that *pezo-1* encodes a mechanosensitive channel. Our findings reveal that *pezo-1* is a mechanosensitive ion channel that regulates food sensation in worms.

INTRODUCTION

Mechanosensitive ion channels regulate several physiological processes ranging from osmotic balance in bacteria (Kung, Martinac and Sukharev, 2010), turgor control in plants (Hamilton, Schlegel and Haswell, 2015), touch (Geffeney and Goodman, 2012; Yan *et al.*, 2013; Ikeda *et al.*, 2014; Maksimovic *et al.*, 2014; Ranade *et al.*, 2014; Woo *et al.*, 2014; Chesler *et al.*, 2016), pain (Murthy *et al.*, 2018; Szczot *et al.*, 2018), proprioception (Woo *et al.*, 2015), hearing (Pan *et al.*, 2018), lineage choice (Pathak *et al.*, 2014), and blood pressure regulation in animals (Retailleau *et al.*, 2015; Wang *et al.*, 2016; Rode *et al.*, 2017; Zeng *et al.*, 2018). These channels are ubiquitous, as they transduce mechanical stimuli into electrochemical signals in all kingdoms of life (Kung, Martinac and Sukharev, 2010; Geffeney and Goodman, 2012; Douguet and Honoré, 2019). In 2010, the PIEZO1 and PIEZO2 channels were identified as essential components of distinct, mechanically activated cation channels in mammalian cells (Coste *et al.*, 2010). Since then, many physiological roles have been assigned to these two ion channels (Parpaite and Coste, 2017).

Mammalian PIEZO channels have been associated with several hereditary pathophysiologies (Alper, 2017). Piezo1 gain-of-function (GOF) mutations display slow channel inactivation leading to an increase in cation permeability and subsequent red blood cell dehydration (Zarychanski *et al.*, 2012; Albuisson *et al.*, 2013; Bae *et al.*, 2013; Ma *et al.*, 2018). For instance, the human Piezo1 hereditary mutation R2456H located in the pore domain decreases inactivation and, when substituted by Lys inactivation is completely removed (Bae *et al.*, 2013). Piezo1 global knockouts (KO) are embryonically lethal in mice (Li *et al.*, 2014; Ranade *et al.*, 2014) and cell-specific KOs result in animals with severe defects (Wu, Lewis and Grandl, 2017; Ma *et al.*, 2018). Intriguingly, both Piezo2 KO and GOF mutations are associated with joint contractures, skeletal abnormalities and alterations in muscle tone (Coste *et al.*, 2013; Chesler *et al.*, 2016; Yamaguchi *et al.*, 2019). GOF and loss-of-function (LOF) mutations are useful genetic tools to determine the contribution of PIEZO channels to mechanosensation in various physiological processes and in different animals.

The *C. elegans* genome encodes an ortholog of the Piezo channel family, namely *pezo-1* (wormbase.org v. WS280). Recently, Bai and collaborators showed that *pezo-1* is expressed in several tissues including the pharynx (Bai *et al.*, 2020). The worm's pharynx is a pumping organ that rhythmically couples muscle contraction and relaxation in a swallowing motion to pass food down to the animal's intestine (Keane and Avery, 2003). This swallowing motion stems from a constant low-frequency pumping maintained by pharyngeal muscles and bursts of high-frequency pumping from a dedicated pharyngeal nervous system (Avery and Horvitz, 1989; Raizen, Lee and Avery, 1995; Trojanowski, Raizen and Fang-Yen, 2016; Lee *et al.*, 2017). In mammals, the swallowing reflex is initiated when pressure receptors in the pharynx walls are stimulated by food or liquids, yet the identity of the receptor(s) that directly evoke this mechanical response remain to be identified (Tsujimura *et al.*, 2019). Interestingly, the *Drosophila melanogaster* PIEZO ortholog is a mechanosensitive ion channel (Kim *et al.*, 2012) required for feeding while also avoiding food over-consumption (Min *et al.*, 2020; Wang *et al.*, 2020). To date, whether *pezo-1* encodes for a mechanosensitive ion channel or regulates worm's pharyngeal activity has yet to be determined.

Here, we found a strong and diverse expression of the *pezo-1* gene in pharyngeal tissues by imaging a *pezo-1::*GFP transgenic reporter strain. By leveraging genetic dissection, electrophysiological measurements, and behavior analyses, we also established that PEZO-1 is required for proper low frequency electric activity and pumping behavior. Analyses of *pezo-1* KO and GOF mutants demonstrated that decreasing or increasing PEZO-1 function upregulates pharyngeal pumping frequency. Likewise, mutants display distinct pharyngeal activities triggered by the neurotransmitter serotonin or with various buffer osmolarities. By using elongated bacteria as a food source, we demonstrated that *pezo-1* KO decreases pharyngeal pumping frequency, whereas the GOF mutant increases it. Finally, electrophysiological recordings of *pezo-1* expressing cells from *C. elegans* embryo cultures and *Spodoptera frugiperda* (Sf9) cell line demonstrate that *pezo-1* encodes a mechanosensitive ion channel. Altogether, our results show that *pezo-1* is a mechanosensitive ion channel involved in a novel biological function regulating pharyngeal pumping and food sensation.

MATERIALS AND METHODS

Strains and Maintenance

Worms were propagated as previously described (Brenner, 1974). N2 (var. Bristol) was referred as wild type (WT) throughout the manuscript. The following strains were used: VVR3 *unc119(ed3)III;decEx1(pRedFlpHgr)(C10C5.1[20789]::S0001_pR6K_Amp_2xTY1ce_EGFP_FRT_rpsl_neo_FRT_3xFlag)dFRT::unc-119-Na*t, COP1553 (KO: 6,616 bp deletion) *pezo-1 (knu508) IV*, COP1524 (GOF: R2373K) *pezo-1 (knu490) IV,* LX960 *lin-15B&lin-15A(n765) X*; *vsIs97 [tph-1p::DsRed2 + lin-15(+)],* DA572 *eat-4(ad572) III,* and DA1051 *avr-15(ad1051) V*. Transgenic strain VVR3 was obtained by microinjecting a fosmid construct (from the TransgeneOme Project) in a *unc-119(ed3)* strain from InVivo Biosystems. COP1553 and COP1524 were obtained using the CRISPR-Cas9 method (InVivo Biosystems). Transgenic worm VVR3 expressing GFP under the control of *Ppezo-1::GFP* was crossed with *pezo-1* mutants COP1553 and COP1524 to obtain VVR69 and VVR70, respectively. LX960 was kindly provided by Dr. Kevin Collins (University of Miami).

Imaging

Worms were selected individually and dropped in 15 µL of M9 buffer (86 mM NaCl, 42 mM Na_2HPO_4, 22 mM KH_2PO_4, 1mM $MgSO_4$) paralyzed on a glass slide containing 2% agarose pads containing 150 mM 2,3-butanedione monoxime (BDM). Bright field and fluorescence imaging were done on a Zeiss 710 Confocal microscope using either a 20X or 40X objective. Images were processed using Fiji ImageJ (Schindelin *et al.*, 2009) to enhance contrast and convert to an appropriate format.

Worms' synchronization

For all pharyngeal pumping assays, worms were synchronized by picking young adults onto fresh nematode growth media (NGM) plates seeded with *E coli* strain OP50 and left to lay eggs for two hours at 20°C. Then, the adults were removed, and the plates incubated at 20°C for three days.

Pharyngeal pumping

Serotonin profile. A serotonin aliquot (InVivo Biosystems) was diluted in M9 Buffer prior to experiments and discarded after three hours. 42 synchronized worms were picked and transferred in 200 µL of M9 Buffer supplemented with 2-, 5-, 10- or 20-mM serotonin and incubated at 20°C for 30 minutes before being loaded inside the microfluidic chip (SC40, The ScreenChip™ System, InVivo Biosystems).

Control E. coli *assay*. OP50 was grown in liquid LB medium under sterile conditions at 37°C and diluted to an optical density of 1.0. Bacterial cultures were stored at 4°C for up to a week.

Spaghetti-like E. coli *assay.* OP50 colonies were picked from a fresh LB plate and incubated in 2 mL of LB overnight the day before the experiment. The following day, 0.5 mL of the pre-incubation culture was used to inoculate 1.5 mL of LB media and grown until growth was exponential, which was verified by checking optical density (optical density of 0.5). Cephalexin (Alfa Aesar™) was then added at 60 µg/ml final concentration and the culture was incubated for two hours. Spaghetti-like OP50 were verified under a microscope and washed three times using 2 mL of M9 buffer followed by centrifugation at 400 *g* to gently pelletize the elongated bacteria.

Pharyngeal recordings and Analyses. Worms were loaded one-by-one inside the microfluidic chip recording channel and left to adjust for one minute prior to recording. All recordings were two minutes long. Records were analysed using NemAnalysis software (InVivo Biosystems) with the brute force algorithm turned off. Parameters were adjusted for each record in order to include the maximum numbers of clearly identifiable pharyngeal pumps. Results were exported from the software in sheet form and parameters were plotted and statistically analysed using MATLAB R2019a (MathWorks).

Development assay

Young adults were allowed to lay eggs on NGM plates seeded with control or spaghetti-like bacteria for two hours. Spaghetti-like bacteria were cultured as described above. Animals (10-20

142 worms) were removed for plates after two hours and the number of eggs laid was counted. After 3
143 days of incubation, animals that reached adulthood were counted in each trial, and results were
144 compared across four trials.

145 **Food ingestion assay**

146 A drop of fresh cultured of control or spaghetti-like bacteria with 2 µM DiI dye (Sigma, CAS
147 #41085-99-8) was placed on a NGM agar plate. Young adults were fed bacteria with DiI for 30 min.
148 Worms were transferred into OP50 seeded NGM without dye for 5 min (Vidal-Gadea *et al.*, 2012).
149 Animals were placed in a thin-layered BDM-agarose plate for imaging under a Nikon SMZ18
150 stereomicroscope. Food occupation in the digestive tract was detected by fluorescence.

151 **Primary culture of *C. elegans* embryo cells**

152 *C. elegans* embryonic cells were generated as previously described (Strange, Christensen and
153 Morrison, 2007). Worms were grown on 10 cm enriched peptone plate with NA22 *E. coli*. NA22
154 bacteria grow in very thick layers that provide abundant food source for large quantities of worms.
155 The synchronized gravid hermaphrodites were bleached to release eggs and washed with sterile egg
156 buffer (118 mM NaCl, 48 mM KCl, 2 mM $CaCl_2$, 2 mM $MgCl_2$, 25 mM HEPES, pH 7.3, 340 mOsm,
157 adjusted with sucrose). The isolated eggs were separated from debris by centrifugation in a 30%
158 sucrose solution. Chitinase (1 U/ml, Sigma) digestion was performed to remove eggshells. The embryo
159 cells were dissociated by pipetting and filtered through a sterile 5µm Durapore filter (Millipore). The
160 cells were plated on glass coverslips coated with peanut lectin solution (SIGMA; 0.5 mg/ml) and
161 cultured in L15 media (Gibco) supplemented with 50 U/ml penicillin, 50 µg/ml streptomycin with
162 10% fetal bovine serum (FBS, Invitrogen) for 72-96 hrs.

163 **Expression of *pezo-1* in Sf9 insect cells**

164 We generated a baculovirus construct consisting of an 8× histidines-maltose binding protein
165 (MBP) tag over *pezo-1* isoform G synthesized nucleotide sequence (one of the longest isoforms

166 according to RNA sequencing, wormbase.org v. WS280). We infected Sf9 cells with the *pezo-1*
167 containing baculovirus for 48 hours. Infected cells were plated on glass coverslips coated with a peanut
168 lectin solution (SIGMA; 0.5 mg/ml) for patch-clamp experiments.

169 **Electrophysiology and mechanical stimulation**

170 Primary cultured embryo cells labeled with *Ppezo-1::GFP* from strains VVR3, VVR69, or
171 VVR70 were recorded in the cell-attached configuration of the patch clamp technique. Control and
172 infected Sf9 insect cells were recorded in the whole-cell patch clamp configuration. For on-cell
173 recordings, the bath solution contained 140 mM KCl, 6 mM NaCl, 2 mM $CaCl_2$, 1 mM $MgCl_2$, 10 mM
174 glucose, and 10 mM HEPES (pH 7.4; 340 mOsm, adjusted with sucrose). The pipette solution
175 contained 140 mM NaCl, 6 mM KCl, 2 mM $CaCl_2$, 1 mM $MgCl_2$, 10 mM glucose, and 10 mM HEPES
176 (pH 7.3; 330 mOsm, adjusted with sucrose). Pipettes were made out of borosilicate glass (Sutter
177 Instruments) and were fire-polished before use until a resistance between 3 and 4 MΩ was reached.
178 Currents were recorded at a constant voltage (-60 mV, unless otherwise noticed), sampled at 20 kHz,
179 and low pass filtered at 2 kHz using a MultiClamp 700B amplifier and Clampex (Molecular Devices,
180 LLC). Leak currents before mechanical stimulations were subtracted offline from the current traces.
181 Cells were mechanically stimulated with negative pressure applied through the patch pipette using a
182 High-Speed Pressure Clamp (ALA Scientific) automated using a MultiClamp 700B amplifier through
183 Clampex (Molecular Devices, LLC). Cell-attached patches were probed using a square-pulse protocol
184 consisting of -10 mmHg incremental pressure steps, each lasting 1 s in 10 s intervals. Cells which giga-
185 seals did not withstand at least six consecutive steps of mechanical stimulation were excluded from
186 analyses. I_{steady} was defined as the maximal current in the steady state. Deactivation was compared by
187 determining the percentage of I_{steady} left 100 ms after the mechanical stimuli ended.

188 For whole-cell recordings, the bath solution contained 140 mM NaCl, 6 mM KCl, 2 mM $CaCl_2$,
189 1 mM $MgCl_2$, 10 mM glucose, and 10 mM HEPES (pH 7.4). The pipette solution contained 140 mM
190 CsCl, 5 mM EGTA, 1 mM $CaCl_2$, 1 mM $MgCl_2$, and 10 mM HEPES (pH 7.2). For indentation assays,

Sf9 cells were mechanically stimulated with a heat-polished blunt glass pipette (3–4 µm) driven by a piezo servo controller (E625, Physik Instrumente). The blunt pipette was mounted on a micromanipulator at an ~45° angle and positioned 3–4 µm above from the cells without indenting them. Displacement measurements were obtained with a square-pulse protocol consisting of 1 µm incremental indentation steps, each lasting 200 ms with a 2 ms ramp in 10 s intervals. Recordings with leak currents >200 pA, with access resistance >10 MΩ, and cells which giga-seals did not withstand at least five consecutive steps of mechanical stimulation were excluded from analyses.

Data and fits were plotted using OriginPro (from OriginLab). Sigmoidal fit was done with the following Boltzmann equation:

Eq. 1: $$f_{(x)} = A_2 + \frac{A_1 - A_2}{1 + e^{(X - X_o)/dX)}}$$

where A_2 = final value, A_1 = initial value; X_o = center, and dX = time constant.

Data and Statistical analyses

Data and statistical analyses were performed using DataGraph 4.6.1, MATLAB R2019a (MathWorks), and GraphPad Instat 3 software. Statistical methods and sample numbers are detailed in the corresponding figure legends. No technical replicates were included in the analyses.

RESULTS

pezo-1 is expressed in a wide variety of cells in the worm's pharynx

To determine the expression of *pezo-1* in *C. elegans*, we used a fluorescent translational reporter made by the TransgeneOme Project (Hasse, Hyman and Sarov, 2016). This fosmid construct contains *pezo-1* native cis-regulatory elements, including introns, up to exon 17 and 3' UTR sequences linked in-frame to the green fluorescent protein (GFP; Figure 1A). The position of the GFP with respect to the remainder of the gene creates an unnatural truncated version of the PEZO-1 protein. Hence, it likely expresses a non-functional protein that misses 16 exons containing the majority of the *pezo-1* sequence (including the pore domain). GFP signals are present in all developmental stages and multiple cells (Supplementary Figure 1A-B), and it does not appear to be mosaic as similar expression patterns were observed in at least three independent transgenic lines. We imaged *pezo-1::*GFP worms at different focal planes to identify the different cells expressing GFP based on their morphological features (i.e., cell-bodies position, neurites extension and positions along the body, and branching). The strongest GFP signals that we identified come from the pharyngeal gland cells (Figure 1B, bright and fluorescence fields). These cells are composed of five cell bodies (two ventral g1s, one dorsal g1 and two ventral g2s) located inside the pharynx terminal bulb and three anterior cytoplasmic projections: two shorts that are superposed ending in the metacorpus and a long one reaching the end of the pm3 muscle. These cells are proposed to be involved in digestion (Albertson and Thomson, 1976; Ohmachi *et al.*, 1999), lubrication of the pharynx (Smit, Schnabel and Gaudet, 2008), generation and molting of the cuticle (Singh and Sulston, 1978; Höflich *et al.*, 2004), and resistance to pathogenic bacteria (Höflich *et al.*, 2004). Additionally, we visualized, *pezo-1::GFP* in a series of cells surrounding the muscle of the corpus and the isthmus (Figure 1C) whose morphology and location match with those of the arcade cells; these were previously hypothesized to be support cells (Albertson and Thomson, 1976). We also recognized as putative *pezo-1* expressing cells: glial cell AmSh, pharyngeal interneuron I3 (Figure 1D), and $M3_{L/R}$ somas and neurites (Figure 1E-F). These neurons

232 are involved in pharyngeal pumping relaxation (Avery, 1993). The finger-like structure known as the
233 pharyngeal sieve, at the junction between corpus and isthmus, also expresses *pezo-1* (Figure 1F).

234 By crossing *pezo-1::GFP* with a *tph-1*::DsRed marker carrying strain, we were able to identify
235 *pezo-1* expression in the pharyngeal $NSM_{L/R}$ secretory, motor, and sensory neurons (Figure 1G).
236 Importantly, these serotoninergic neurons have been proposed to sense food in the lumen of the
237 pharynx through their proprioceptive-like endings and trigger feeding-related behaviors (i.e., increased
238 pharyngeal pumping, decreased locomotion, and increased egg laying) (Albertson and Thomson,
239 1976; Avery, Bargmann and Horvitz, 1993). In addition to the pharyngeal cells, we observed
240 expression of *pezo-1* in the ventral nerve cord (VNC, Figure 1D) neurons, striated muscles
241 (Supplementary Figure 1C), coelomocytes (Supplementary Figure 1D-E), spermatheca
242 (Supplementary Figure 1B and 1E), vulval muscles (Supplementary Figure 1F), and various male
243 neurons including the ray neurons (Supplementary Figure 1G). Importantly, the expression pattern
244 reported by our *pezo-1* fosmid construct matches very well with the gene expression atlas for *C.*
245 *elegans* neurons (Taylor *et al.*, 2020), except for the M3 neurons. The strong and varied *pezo-1*
246 expression in the pharynx along with the function of the cells expressing it, led us to investigate the
247 potential contribution of PEZO-1 to pharyngeal function.

248

249

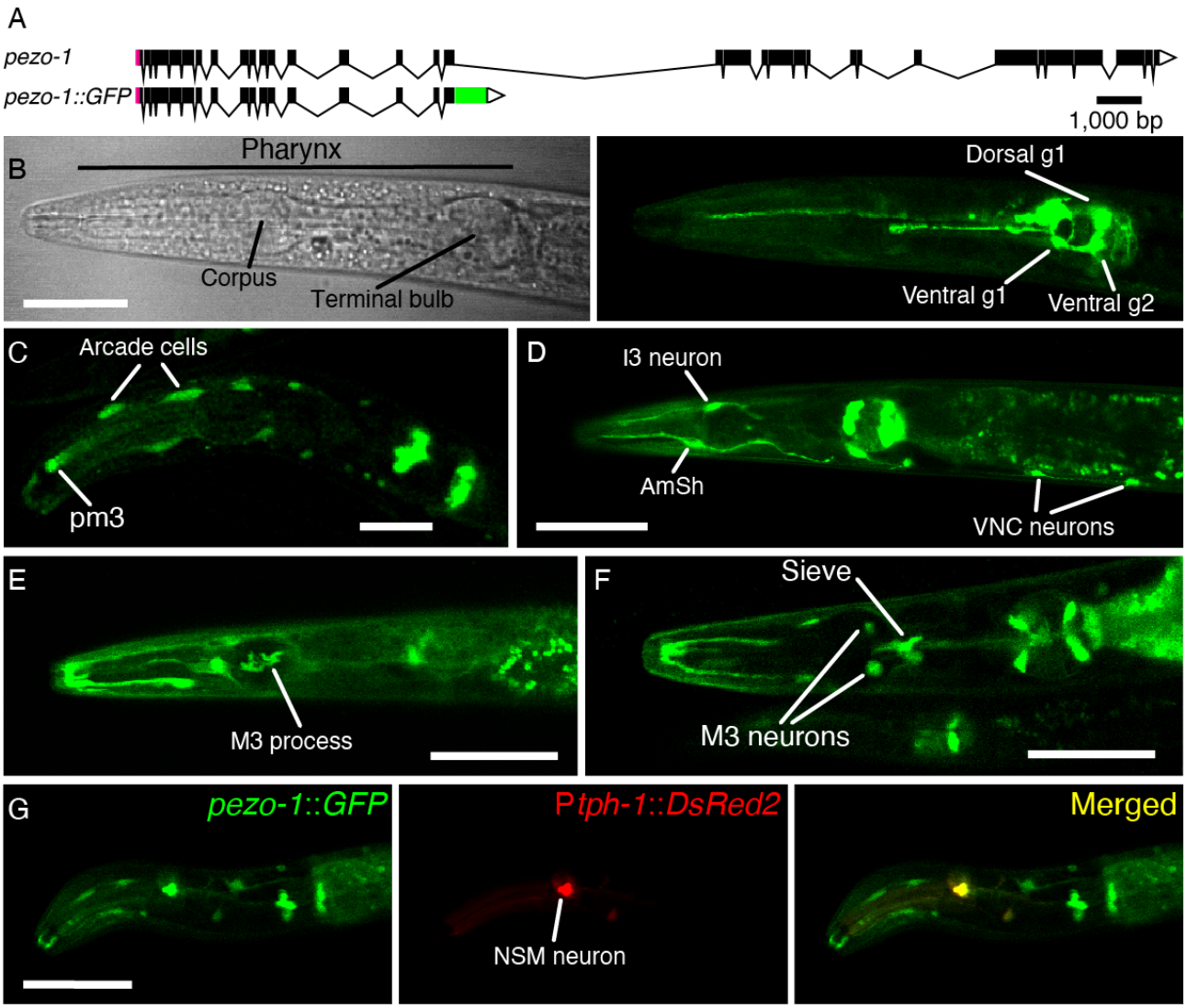

Figure 1. *pezo-1* is strongly expressed in *C. elegans* pharynx. (**A**) *pezo-1* gene diagram according to wormbase.org, v. WS280 made with Exon-Intron Graphic Maker http://wormweb.org/. Magenta rectangles and white triangles denote the 5' and 3' untranslated regions (UTR), respectively. Black rectangles denote exons and black lines denote introns. Green rectangle denotes the GFP sequence inserted after exon 17. (**B**) Brightfield (left) and fluorescence (right) micrographs of the anterior end of a young adult *pezo-1*::GFP hermaphrodite highlighting pharynx structures and the GFP reporter expression in gland cells. Scale bar represents 50 µm. (**C**) Micrograph of the anterior end of a young adult *pezo-1*::GFP hermaphrodite expressing GFP in cells identified as arcade and pharyngeal muscle cells (pm3), according to their position. Scale bar represents 20 µm. (**D-E**) Micrograph of the anterior end of a young adult *pezo-1*::GFP hermaphrodite expressing GFP in cells identified as neurons (I3, M3, VNCs) and sheath cell (AmSh), according to their position. Scale bar represents 50 µm. (**F**) Micrograph of the anterior end of a young adult *pezo-1*::GFP hermaphrodite expressing GFP in cells identified ad M3 and pharyngeal sieve, according to their position. Scale bar represents 100 µm. (**G**) Co-localization between *tph-1*::DsRed2 and *pezo-1*::GFP reporter in the neuron NSM. Scale bar represents 50 µm. Micrographs are representative of at least 20 independent preparations.

Serotonin stimulation reveals different pharyngeal pump parameters

To analyze the contribution of *pezo-1* to pharyngeal pumping in *C. elegans*, we used the ScreenChip^{TM} system (InVivo Biosystems) that allows measuring electropharyngeogram recordings (EPG; Figure 2A) (Raizen and Avery, 1994) by loading single-live worms inside a microfluidic chip. Figure 2A-B summarizes the pharynx anatomy, electrical properties measured during an EPG, and the neurons involved in pharyngeal function. For instance, the excitation event (E spike) precedes the pharyngeal contraction and is modulated by the pacemaker neuron MC (Figure 2B, top), whereas the repolarization event (R spike) leads to pharyngeal relaxation and correlates to the activity of the inhibitory M3 motorneurons (Figure 2B, middle). Every 3-4 pumps, there is relaxation of the terminal bulb (isthmus peristalsis) which is modulated by the motorneuron M4 (Figure 2B, bottom) (Avery and Horvitz, 1989). The main EPG events are regulated by the pharyngeal proprioceptive neuron NSM. Importantly, M3 motorneurons (potentially) and the NSM proprioceptive neuron express *pezo-1* (Figure 1E-G).

Analyses of the EPG records allow determination of different pharyngeal pumping parameters including frequency, duration, and the time interval that separates two pumping events (hereafter referred to as the interpump interval). We used serotonin to increase pharyngeal activity since, in the absence of food or serotonin, the pumping events are infrequent. Serotonin mimics food stimulation by activating the $MC_{L/R}$ and $M3_{L/R}$ neurons (Niacaris, 2003). First, we established a serotonin dose-response profile of the WT strain pharyngeal pumping parameters (N2; Figure 2C-G). Serotonin increases pharyngeal pumping frequency in a dose-dependent manner, with concentrations above 5 mM increasing the likelihood of reaching 5 Hz (Figure 2C). We averaged the EPG recordings at each serotonin concentration and found a clear difference in pump durations between 0- and 5-mM. Concentrations equal or higher than 5 mM evoke similar pump durations (~100 ms; Figure 2D). Interestingly, analyses of the pump duration distribution profile under serotonin stimulation revealed that pharyngeal pump duration fits into two categories: fast (~80 ms) and slow (100-120 ms; Figure

2E; gray rectangles).

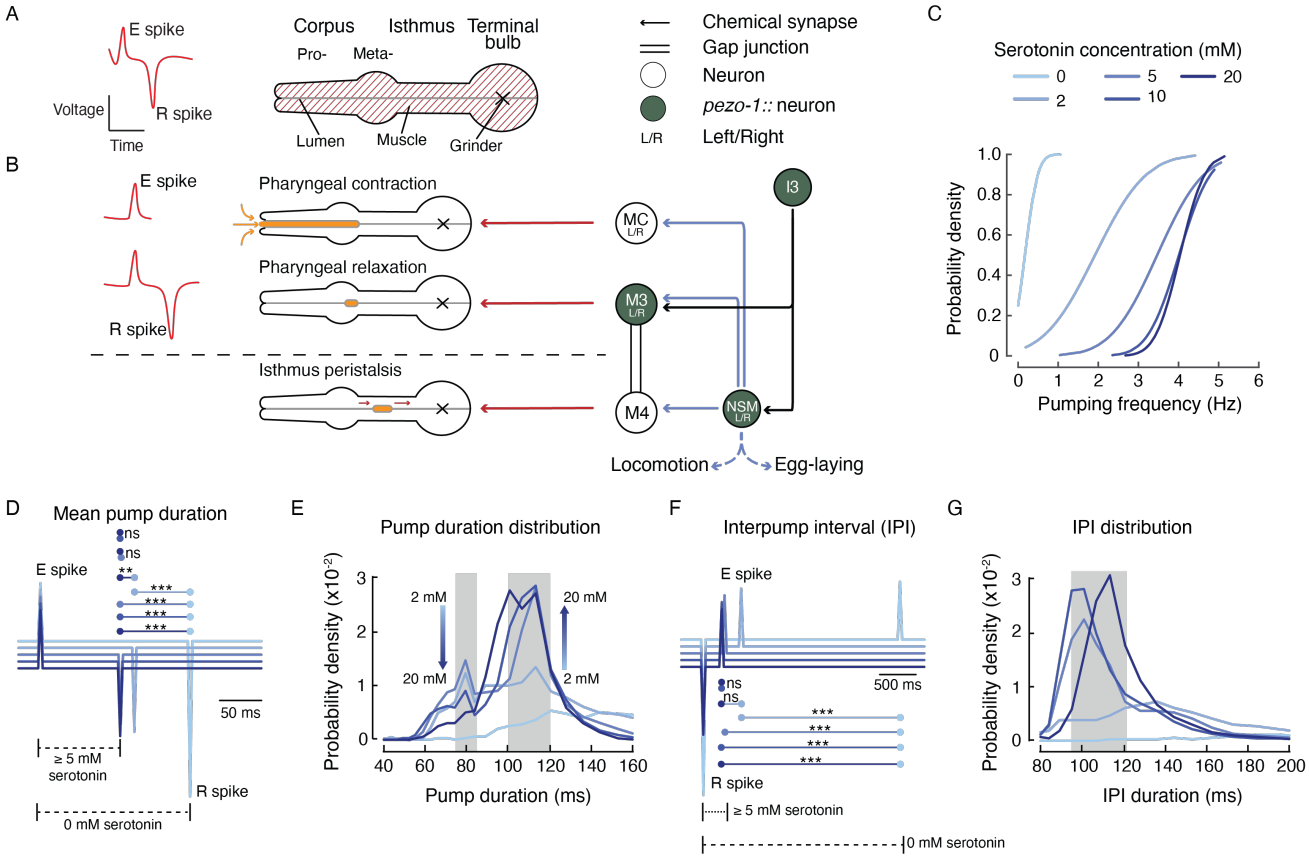

Figure 2. Serotonin triggers pharyngeal pumping in a concentration-dependent manner in WT (N2) worms. (**A**) Left, illustration of an electropharyngeogram (EPG) recording depicting the contraction-relaxation of the corpus, referred to as a pharyngeal pump. Right, illustration representing *C. elegans* pharyngeal muscle. (**B**) Representation of the main pharyngeal electrical coupling in *C. elegans*. Blue arrows represent serotoninergic transmission, red arrows represent neuromuscular junction, double lines represent gap junction, filled circles represent neurons putatively expressing of *pezo-1*, open circles represent neurons not expressing *pezo-1*. (**C**) Probability densities for pharyngeal pumping frequencies at different serotonin concentrations. Results for every serotonin concentration were statistically compared by Kolmogorov-Smirnov test (*p*-values are shown in Table I). n is 90 worms per condition. (**D**) Ensemble averages of EPG traces for different serotonin concentrations showing pump durations (E to R spikes). One-way ANOVA and Tukey-Kramer multiple comparisons test. n is 90 worms per condition (**E**) Serotonin concentration effect on pump duration. A kernel probability distribution was fit to the data. n is 90 worms per condition. (**F**) Ensemble averages of EPG traces for different serotonin concentrations showing interpump interval (R to E spikes). One-way ANOVA and Tukey-Kramer multiple comparisons test. n is 90 worms per condition (**G**) Serotonin concentration effect interpump interval. A kernel probability distribution was fit to the data. n is 90 worms per condition. Asterisks indicate values significantly different (***$p < 0.001$ and **$p < 0.01$) and ns indicates not significantly different.

We observed that the fast and slow categories displayed an inverse relationship with respect to serotonin concentration (Figure 2E; arrows). We hypothesize that slow (100-120 ms) pumps are the result of the serotoninergic activation of $M3_{L/R}$ while the fast (~ 80 ms) pumps originate from a

mechanism that is partly independent from the serotonin pathway. Unlike pump duration, we observed only one category for interpump intervals around 95-120 ms for 5- to 20-mM serotonin concentrations (Figure 2F-G). Interestingly, we did not observe inter pump intervals faster than 90 ms, regardless of the serotonin concentration. The inter pump intervals results support the idea that there is a minimum refractory period between two pumps. This set of analyses allowed us to establish a suitable model for evaluating the role of *pezo-1* function *in vivo*.

***pezo-1* mutants display higher pumping frequency than WT worms**

To determine whether *pezo-1* has a functional role in pharyngeal pumping, we engineered LOF and GOF mutants. A putative LOF mutant obtained by deleting 6,616 bp from the *pezo-1* locus (hereafter referred to as *pezo-1* KO; Figure 3A, top). Previous works demonstrated that the substitution of R2456H (located at the pore helix) of the ortholog human *Piezo1* gene increases cation permeability (GOF) and causes hemolytic anemia (Zarychanski *et al.*, 2012; Albuisson *et al.*, 2013; Bae *et al.*, 2013). Moreover, a conservative substitution of Lys for Arg at position 2456 in the human *Piezo1* channel exhibits a pronounced decreased inactivation when compared to the WT or R2456H channels (Bae *et al.*, 2013). Hence, we engineered a putative GOF mutant strain obtained by substituting the conserved Arg 2373 with Lys (hereafter referred to as *pezo-1* R2373K or GOF; Figure 3A, bottom). Parenthetically, the R2373K numbering position is based on isoform G – one of the longest isoforms according to RNA sequencing (wormbase.org v. WS280). We also included in our analysis two mutants known to alter pharyngeal function, *eat-4(ad572)* and *avr-15(ad1051)*. EAT-4 is a glutamate-sodium symporter involved in postsynaptic glutamate reuptake. *eat-4(ad572)* affects the neurotransmission efficiency of all glutamatergic pharyngeal neurons ($I2_{L/R}$, I5, $M3_{L/R}$, M4, MI, $NSM_{L/R}$) (Lee *et al.*, 1999). AVR-15 is a glutamate-gated chloride channel expressed in the pharyngeal muscle pm4 and pm5 (both synapsed by $M3_{L/R}$) and involved in relaxation of the pharynx. Its mutant allele *ad1051* lengthen pump duration by delaying relaxation of the pharynx in a similar fashion as laser ablation of $M3_{L/R}$ neurons (Dent, Davis and Avery, 1997). With these strains, we sought to determine if altering PEZO-1 function would affect the worm's pharyngeal phenotype.

307 At 2 mM concentration of exogenous serotonin (to elicit pharyngeal activity), both *pezo-1* KO
308 and R2373K mutants displayed significantly higher pumping frequencies than WT and similar to *avr-*
309 *15(ad1051)* (Figure 3B). On the other hand, the *eat-4(ad572)* mutant displayed lower pumping
310 frequency at this serotonin concentration. To further assess the *pezo-1* mutants' pharyngeal altered
311 function, we analyzed the pump duration distributions from the EPG records. *pezo-1* KO distribution
312 is similar to the WT (Figure 3C, red *vs.* black) whereas the R2373K mutant profile is reminiscent of
313 the *avr-15(ad1051)*, as both mutant strains displayed a narrower distribution around 100 ms pump
314 events (Figure 3C, blue and green *vs.* black). Moreover, the R2373K mutant lacked fast pump events
315 between 50 to 80 ms (Figure 3C, blue bracket), similar to the WT features observed at high serotonin
316 concentrations (≥ 5 mM, Figure 2E), and the *eat-4(ad572)* mutant and the *avr-15(ad1051)* mutant at
317 2 mM serotonin concentration (Figure 3C, yellow and green brackets). The analysis of distribution of
318 interpump intervals revealed that *pezo-1* KO and R2373K mutants, although different, both spend less
319 time resting between pumps (95-120 ms) than the WT (≈ 140 ms) (Figure 3D, red and blue brackets).
320 This enhancement in function resembles the WT activity measured at 5- to 20-mM serotonin
321 concentrations (Figure 2F-G) and could account for the increase in frequency shown in Figure 3B. The
322 close resemblance between the PEZO-1 GOF and the *avr-15(ad1051)* mutants' pharyngeal pumping
323 parameters suggests a potential link between PEZO-1 and pharyngeal relaxation through $M3_{L/R}$
324 neurotransmission.

325

326

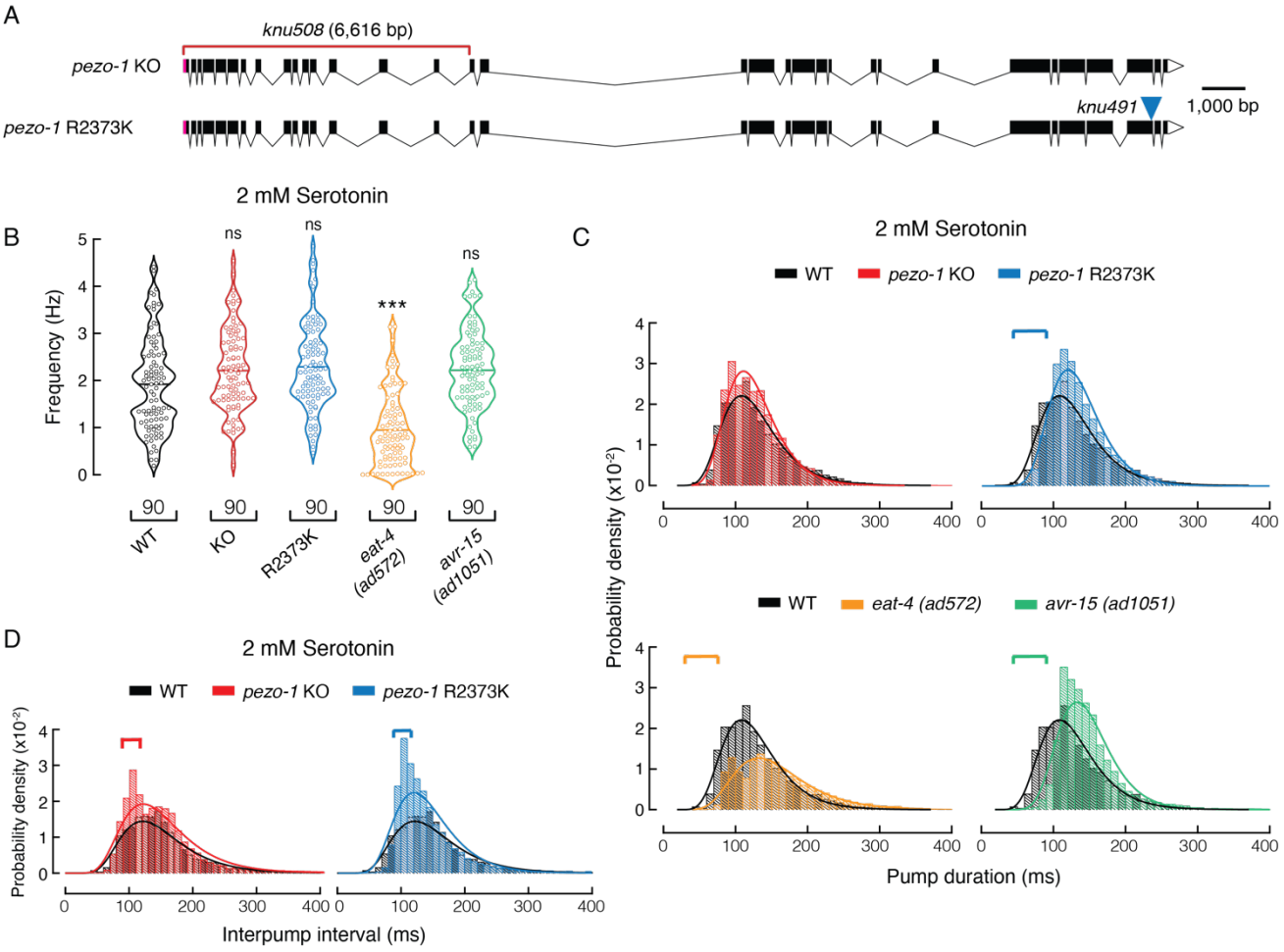

Figure 3. PEZO-1 activation affects pharyngeal pumping properties at 2 mM serotonin. (**A**) *pezo-1* gene diagram according to wormbase.org v. WS280 made with Exon-Intron Graphic Maker WormWeb.org. Magenta rectangles and white triangles denote the 5' and 3' untranslated regions (UTR), respectively. Black rectangles denote exons and black lines denote introns. The red bracket denotes the *knu508* allele (a 6,616bp deletion) of the *pezo-1* KO strain and the blue triangle denotes the single point mutation (allele *knu491*) of the *pezo-1* R2373K strain. (**B**) Pharyngeal pumping frequencies depicted as violin plots with the means shown as horizontal bars for WT (N2), *pezo-1* KO, *pezo-1* R2373K, *eat-4 (ad572)*, and *avr-15 (ad1051)* strains. n is denoted above the *x*-axis. Kruskal-Wallis and Dunn's multiple comparisons tests. Asterisks indicate values significantly different (***$p < 0.001$) and ns indicates not significant. (**C**) Comparison between WT and *pezo-1* KO, *pezo-1* R2373K, *eat-4 (ad572)*, and *avr-15 (ad1051)* strains pump duration distribution histograms. Smooth curves were fit to the data according to a log-normal distribution. Number of events ≥ 20,860; bin size 30. n is 90 worms per condition. (**D**) Comparison between WT, *pezo-1* KO, and *pezo-1* R2373K strains interpump interval distribution histograms, at 2 mM serotonin concentration. Smooth curves were fit to the data according to a log-normal distribution. Number of events ≥ 10,200; bin size 30. n is 90 worms per condition.

329 **PEZO-1 determines pharyngeal pumping in response to hyperosmolarity**

330 Mechanical stimuli come in many forms including stretching, bending, and osmotic forces
331 (Cox, Bavi and Martinac, 2019). To further understand the functional role of *pezo-1*, we evaluated
332 pharyngeal pumping parameters after challenging worm strains with different osmolarities. To this
333 end, we diluted the standard solution used for worm experiments (M9 buffer) to different osmolarities
334 (150, 260, and 320 mOsm). Low osmolarity solutions would be equivalent to swallowing food
335 containing few solutes (150 mOsm) whereas high osmolarities would represent a "gulp" with large
336 amounts of solutes (320 mOsm). Noteworthy, the higher the osmolarity, the shorter the mean pumping
337 frequency of WT worms (Figure 4A). Our results indicate that the larger the number of solutes in
338 solution, the longer they would reside in the pharynx before moving to the intestine. Notably, at 320
339 mOsm, both *pezo-1* KO and GOF mutants displayed a significantly higher frequency than WT (Figure
340 4A). On the other hand, at 260 and 150 mOsm we did not measure significant differences between WT
341 and the *pezo-1* mutants. Similar to human Piezo2 KO and GOF mutations (associated with joint
342 contractures), we demonstrated that lack of or enhanced PEZO-1 function modulated pharyngeal
343 pumping frequencies in the same fashion (at high osmolarities). Next, we further examined the EPG
344 parameters at high osmolarity (320 mOsm). Analyses of the distribution of pump durations and length
345 of the mean interpump intervals revealed that both *pezo-1* mutants had more frequent fast pumps (80-
346 120 ms, Figure 4B, gray rectangles) and spent less time resting between pumps than the WT (Figure
347 4C). Interestingly, high osmolarity (320 mOsm) revealed a close resemblance between PEZO-1 GOF
348 and the *avr-15(ad1051)* mutants' pharyngeal pumping parameters (frequency and duration, Figure 4D-
349 E) suggesting a potential link between PEZO-1 and $M3_{L/R}$ function. Altogether, our results suggest
350 that PEZO-1 is required for fine tuning pharyngeal function in response to osmolarity changes.
351

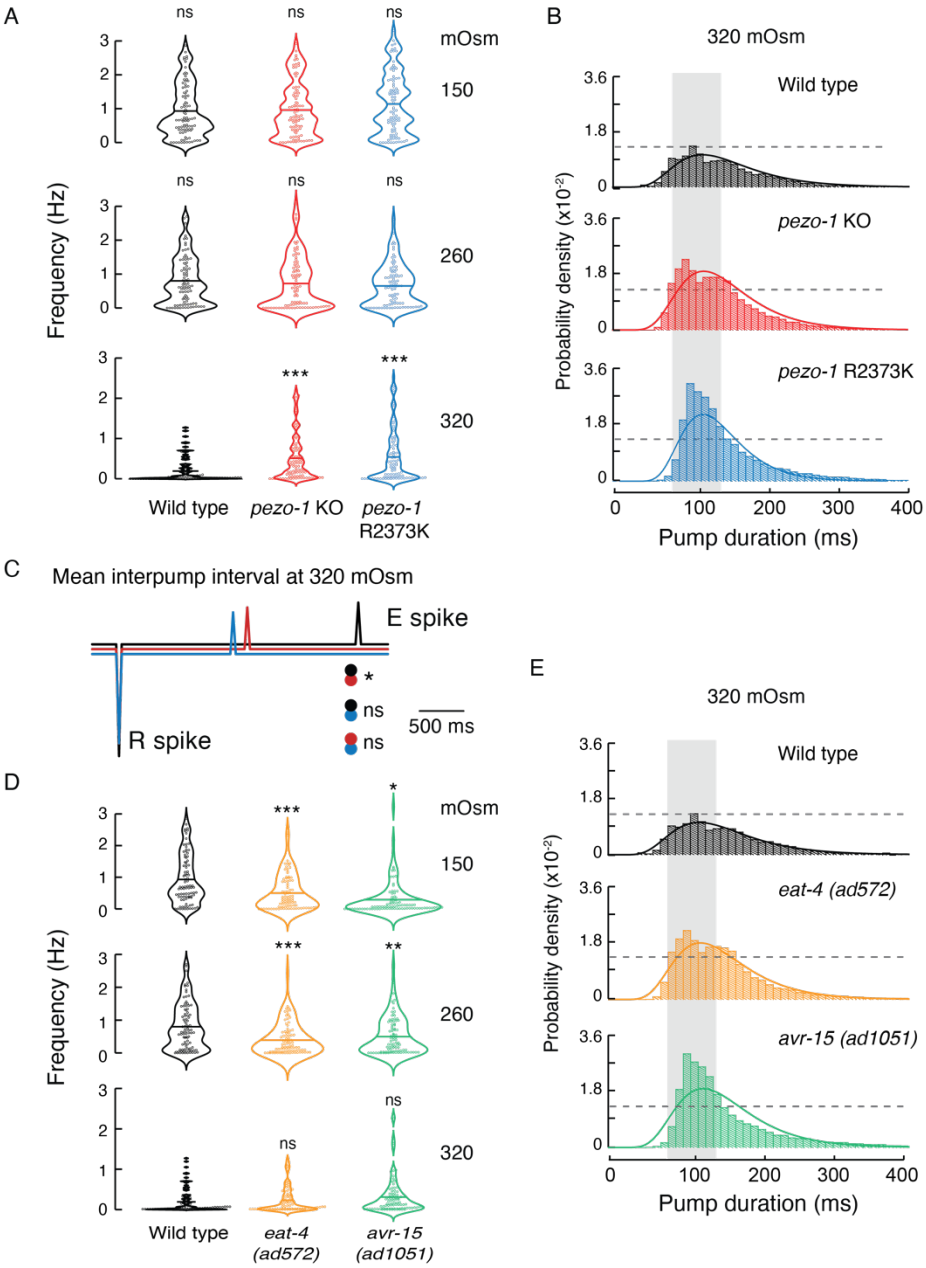

Figure 4. Osmolarity changes modify pharyngeal pumping in WT and *pezo-1* strains. (**A**) Pharyngeal pumping frequencies depicted as violin plots with the means shown as horizontal bars for WT (N2), *pezo-1* KO, and *pezo-1* R2373K strains at 150, 260, and 320 mOsm. n is 90 worms per condition. Kruskal-Wallis and Dunn's multiple comparisons tests. (**B**) Comparison of probability densities for pharyngeal pumping duration of WT, *pezo-1* KO, and *pezo-1* R2373K strains at 150, 260, and 320 mOsm. Smooth curves were fit to the data according to a log-normal distribution. Number of events ≥ 21,110; bin size 30. n is 90 worms per condition. (**C**) Ensemble averages of EPG traces for WT (N2), *pezo-1* KO, and *pezo-1* R2373K strains showing pump durations (E to R spikes) at 320 mOsm. One-way ANOVA and Tukey-Kramer multiple comparisons test. n is 90 worms per condition. (**D**) Pharyngeal pumping frequencies depicted as violin plots with the means shown as horizontal bars for WT (N2), *eat-4 (ad572)*, and *avr-15 (ad1051)* strains at 150, 260, and 320 mOsm. n = 90, per condition. Kruskal-Wallis and Dunn's multiple comparisons tests. (**E**) Comparison of probability densities for pharyngeal pumping duration of WT, *eat-4 (ad572)*, and *avr-15 (ad1051)* strains at 150, 260, and 320 mOsm. Smooth curves were fit to the data according to a log-normal distribution. Number of events ≥ 21,110; bin size 30. n is 90 worms per condition. Asterisks indicate values significantly different (***$p < 0.001$, **$p < 0.01$, and *$p < 0.05$) and ns indicates not significant.

PEZO-1 function is involved in food sensation

To determine the impact that PEZO-1 function has on food intake, we recorded pharyngeal pumping of WT and *pezo-1* strains in response to different food stimuli. It has been hypothesized that food quality and feeding preferences displayed by worms is linked to the bacteria size (Shtonda and Avery, 2006). To this end, we measured worms pharyngeal pumping while feeding them the conventional food used in the laboratory for maintenance (*Escherichia coli* strain OP50). Additionally, we varied the dimensions of OP50 using the antibiotic cephalexin; an antibiotic that prevents the separation of budding bacteria, generating long spaghetti-like filaments of bacterium as observed under a microscope and elsewhere (Martinac *et al.*, 1987) (Supplementary Figure 2A). A similar method was previously described using the antibiotic aztreonam and has been shown to affect pharyngeal pumping (Gruninger, Gualberto and Garcia, 2008; ben Arous, Laffont and Chatenay, 2009).

WT and *pezo-1* mutants are able to ingest spaghetti-like bacteria and reached adulthood in three days, similar to worms fed with control bacteria (Supplementary Figure 2B-C). Notably, feeding worms with control or spaghetti-like bacteria revealed different pharyngeal traits between the *pezo-1* mutants and the WT worms. When fed with control *E. coli*, both *pezo-1* mutants (KO and GOF) have higher mean frequencies, shorter mean pump durations, narrower pump duration distributions, and fastest mean interpump intervals than the WT worms (Figure 5A-C, E-F). On the other hand, feeding worms with spaghetti-like *E. coli* elicits opposite effects on the *pezo-1* mutants pharyngeal pumping parameters. For instance, spaghetti-like *E. coli* decreases *pezo-1* KO mean frequency, while keeping the mean pump duration and distribution similar to WT (Figure 5A-B, D). Furthermore, this modified diet significantly increases the mean interpump interval of the KO in comparison to the WT and the GOF mutant (Figure 5E-F). Unlike the KO and WT, the R2372K *pezo-1* mutant displays high frequency, short pumps (mean and distributions; Figure 5A-B, D) and short mean interpump interval durations (mean and distributions; Figure 5E-F). Altogether, our results indicate that PEZO-1 regulates the pharynx response to food physical parameters, such as length and shape of the ingested bacteria.

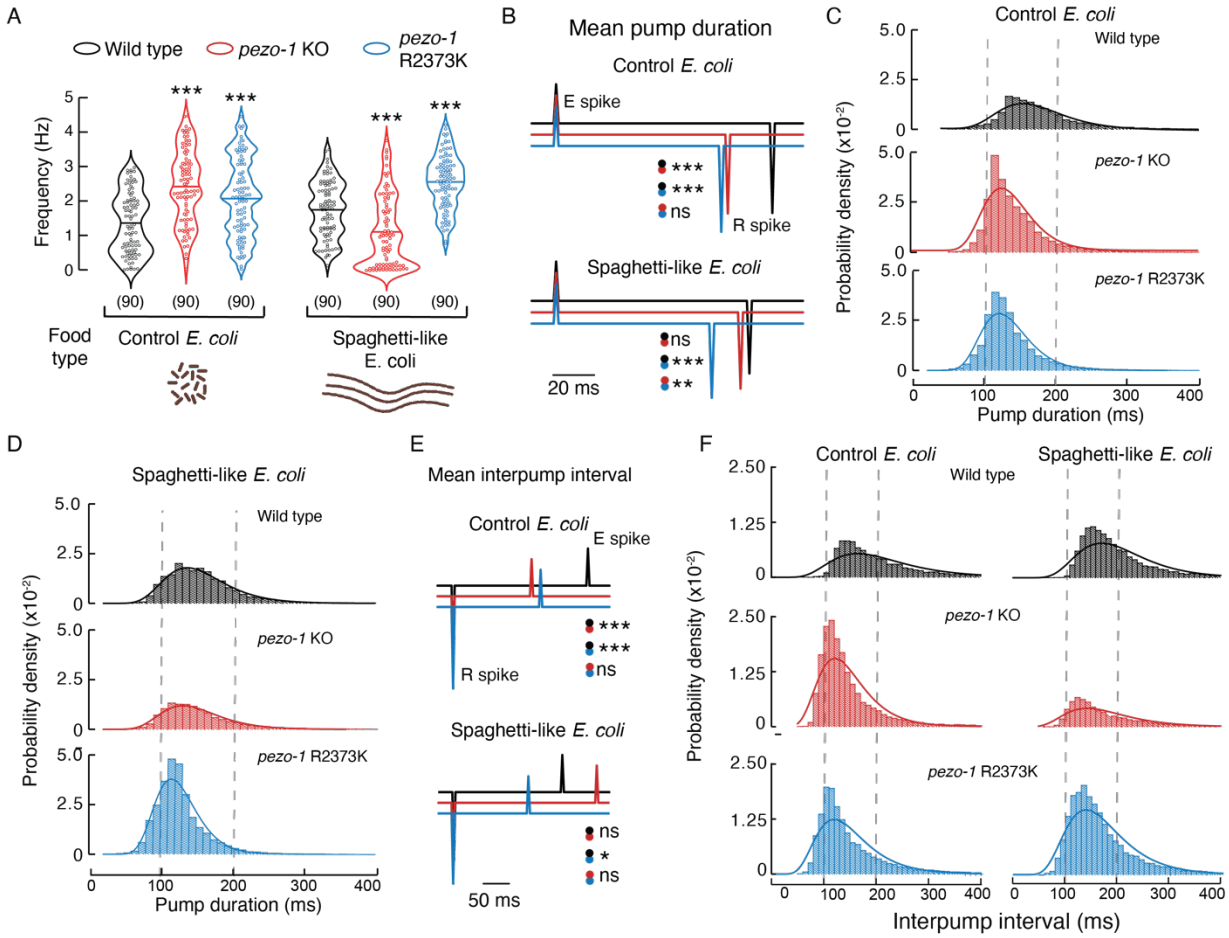

Figure 5. PEZO-1 alters pharyngeal pumping when exposed to control or spaghetti-like bacteria. (**A**) Pharyngeal pumping frequencies depicted as violin plots with the means shown as horizontal bars for WT (N2), *pezo-1* KO, and *pezo-1* R2373K when fed with control and cephalexin-treated bacteria (spaghetti-like *E. coli*) (bacteria cartoons were created with BioRender.com). n is denoted above the *x*-axis. Kruskal-Wallis and Dunn's multiple comparisons tests. Asterisks indicate values significantly different (***$p < 0.001$). (**B**) Ensemble averages of EPG traces for WT (N2), *pezo-1* KO, and *pezo-1* R2373K strains showing pump durations (E to R spikes), when fed with control and cephalexin-treated bacteria (spaghetti-like *E. coli*). One-way ANOVA and Tukey-Kramer multiple comparisons test. n is 90 worms per condition. (**C**) Comparison of probability densities for pharyngeal pump duration of wild-type (N2), *pezo-1* KO, and *pezo-1* R2373K when fed with control bacteria. Smooth curves were fit to the data according to a log-normal distribution. Number of events ≥ 14,740; bin size 30. n is 90 worms per condition. (**D**) Comparison of probability densities for pharyngeal pump durations of WT (N2), *pezo-1* KO, and *pezo-1* R2373K when fed with cephalexin-treated bacteria (spaghetti-like *E. coli*). Smooth curves were fit to the data according to a log-normal distribution. Number of events ≥ 19,160; bin size 30. n is 90 worms per condition. (**E**) Ensemble averages of EPG traces for WT (N2), *pezo-1* KO, and *pezo-1* R2373K strains showing interpump interval (R to E spikes), when fed with control and cephalexin-treated bacteria. One-way ANOVA and Tukey-Kramer multiple comparisons test. n is 90 worms per condition. (**F**) Comparison of probability densities for pharyngeal interpump interval of WT (N2), *pezo-1* KO, and *pezo-1* R2373K when fed with control and cephalexin-treated bacteria. Smooth curves were fit to the data according to a log-normal distribution. Number of events ≥ 9,950; bin size 30. n is 90 worms per condition. Asterisks indicate values significantly different (***$p < 0.001$, **$p < 0.01$, and *$p < 0.05$) and ns indicates not significantly different.

pezo-1 encodes a mechanosensitive ion channel

The PEZO-1 protein sequence shares 60-70% similarity with mammalian PIEZO channel orthologs. However, whether PEZO-1 responds to mechanical stimuli has not yet been established. To address this major question, we generated three different *pezo-1* strains expressing the *pezo-1::*GFP, *pezo-1::*GFP KO, and *pezo-1::*GFP R2373K mutation. *pezo-1::*GFP cells were patch-clamped using the cell-attached configuration while applying constant negative pressure (- 70 mmHg) and steps of positive and negative voltages to the pipette (Figure 6A-C). The current *vs.* voltage relationship is characterized by a reversal potential of + 9.31 mV (Figure 6D), indicating that PEZO-1 mediates a slight cation selective conductance like the mouse and *Drosophila*'s orthologs (Coste *et al.*, 2012).

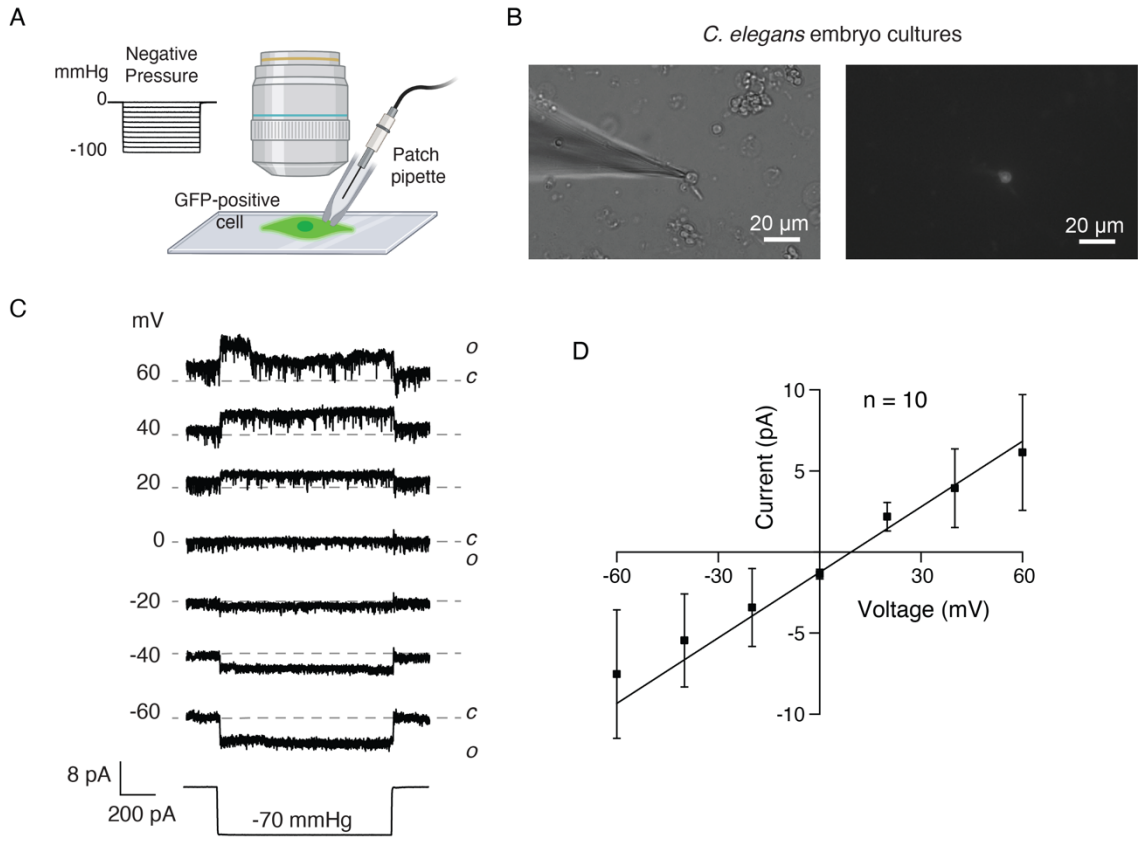

Figure 6. Cells expressing PEZO-1 display mechanosensitive channel currents (**A**) Schematic representation of the mechanical stimulation protocol applied to *pezo-1*::GFP expressing cells recorded in the cell-attached configuration. Created with BioRender.com. (**B**) Representative micrographs (from at least 10 independent preparations) of a *C. elegans* primary embryonic culture from *pezo-1::*GFP expressing strains. Brightfield (left) and fluorescence (right) micrographs of a *pezo-1::*GFP expressing cell when patch clamped in the on-cell configuration. (**C**) Representative cell-attached patch-clamp recordings of mechanically-activated currents from WT, *p*ezo-1 KO, and *pezo-1* R2373K cells expressing *pezo-1::*GFP. Channel openings (downward) were elicited by -70 mmHg square pulse (bottom) at constant voltages ranging from -60 to +60 mV. Gray dashed line represents background currents. Closed and open states are labeled *c* and *o*, respectively. (**D**) Current-voltage relation recorded at a constant pressure of -70 mmHg in the on-cell configuration. The reversal potential is 9.31 mV. Each circle represents the mean ± SD.

Mechanical stimulation of cells expressing WT PEZO-1 elicited mechano-dependent currents (Figure 7A-C, black traces and bar) with a half pressure activation ($P_{1/2}$) corresponding to -59.1 ± 4.3 mmHg (mean ± SEM). Importantly, *pezo-1::GFP* cells expressing KO PEZO-1 did not feature mechanosensitive currents, even at larger negative pressure magnitudes (Figure 7A and C, red traces and bar). On the other hand, PEZO-1 R2373K displayed mechano-dependent currents (Figure 7A-C, blue traces and bar) with lower $P_{1/2}$ than the WT channel (39.2 ± 2.2 mmHg, mean ± SEM), indicating that the GOF mutant requires less mechanical activation to open. Notably, the R2373K mutation introduced a latency for activation that was not detected in the WT (Figure 7A, blue traces and 7D). The decrease in mechanical threshold along with the slow activation were previously reported for the equivalent human PIEZO1 R2456K mutation in mammalian cell lines (Zarychanski *et al.*, 2012; Albuisson *et al.*, 2013; Bae *et al.*, 2013; Romero *et al.*, 2019). Future experiments are needed to understand the origin of these differences in activation. Unlike *pezo-1* WT, approximately 50% of the mechano currents elicited from the *pezo-1* R2373K expressing cells remained active even after the mechanical stimulus ended (Figure 7A, blue traces, and 7E). This slow deactivation is also reminiscent of the human PIEZO1 R2456K GOF phenotype previously characterized by Bae and collaborators (Bae *et al.*, 2013). Overall, our results support that PEZO-1 is an ion channel gated by membrane tension and that a conservative mutation in the pore domain elicits similar activation and kinetic changes as its human counterpart.

To further validate that the *pezo-1* gene encodes for a mechanosensitive ion channel, we heterologously expressed one of the longest isoforms of *pezo-1* (isoform G; wormbase.org v. WS280) in Sf9 cells. Similar to mammalian PIEZO channels, PEZO-1 mediates indentation-activated currents (Figure 8). Uninfected Sf9 cells do not display mechanosensitive channel currents (Figure 8B-C). Importantly PEZO-1 displayed the properties described for mammalian PIEZOs in other cell types including (Coste *et al.*, 2010; Wu *et al.*, 2017) non-selective cation currents, as determined by the reversal potential (+ 6.74 mV; Figure 8D-E) and voltage-dependent inactivation (Figure 8D and 8F). Our results demonstrate that expressing *pezo-1* in a naïve cell was sufficient to confer mechanosensitivity to Sf9 cells.

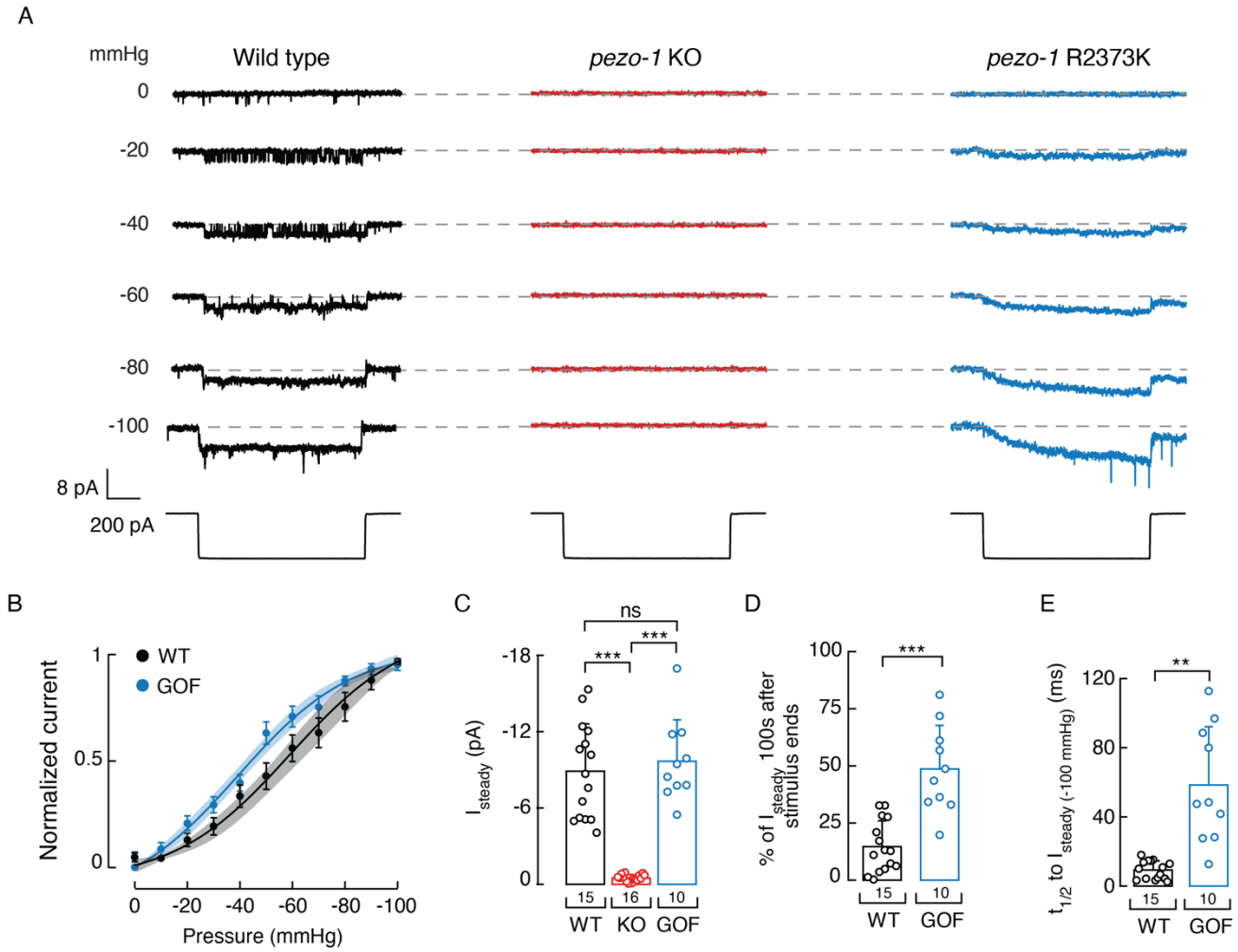

Figure 7. PEZO-1 GOF mutant decreases mechanical threshold and slows down deactivation. (**A**) Representative cell-attached patch-clamp recordings of mechanically-activated currents from WT, *p*ezo-1 KO, and *pezo-1* R2373K cells expressing *pezo-1::*GFP. Channel openings (downward) were elicited by negative pressure (left) square pulses (bottom) at a constant voltage of -60 mV. Gray dashed line represents background currents and channel openings are downward. (**B**) Pressure-response profiles for PEZO-1 WT and R2373K currents. Normalized currents elicited by negative pressure of mechanically activated currents of WT and pezo-1 R2373K cells expressing *pezo-1::*GFP. A Boltzmann function, Eq. (1), was fitted to the data. The shadows below the curves indicate the 95% confidence bands for the fit. Circles are mean ± SD. n for WT and *pezo-1* R2373K are 15 and 10, respectively. (**C**) Bar graph displaying steady state currents elicited by -100 mmHg of negative pressure of WT, *p*ezo-1 KO, and *pezo-1* R2373K cells expressing *pezo-1::*GFP. Bars are mean ± SD. n is denoted above the *x*-axis. Kruskall-Wallis and Dunn's multiple comparisons tests. (**D**) Bar graph displaying the time it takes to reach half of the steady state currents elicited with -100 mmHg of pressure of WT and *pezo-1* R2373K cells expressing *pezo-1::*GFP. Bars are all mean ± SD. n is denoted above the *x*-axis. Unpaired *t*-test with Welch's correction. (**E**) Bar graph displaying percentage of steady state currents left 100 ms after the mechanical stimulus ended of WT and *pezo-1* R2373K cells expressing *pezo-1::*GFP. Bars are mean ± SD. n is denoted above the *x*-axis. Unpaired *t*-test. Asterisks (***$p < 0.001$ and **$p < 0.01$) indicate values significantly different. ns indicates not significant.

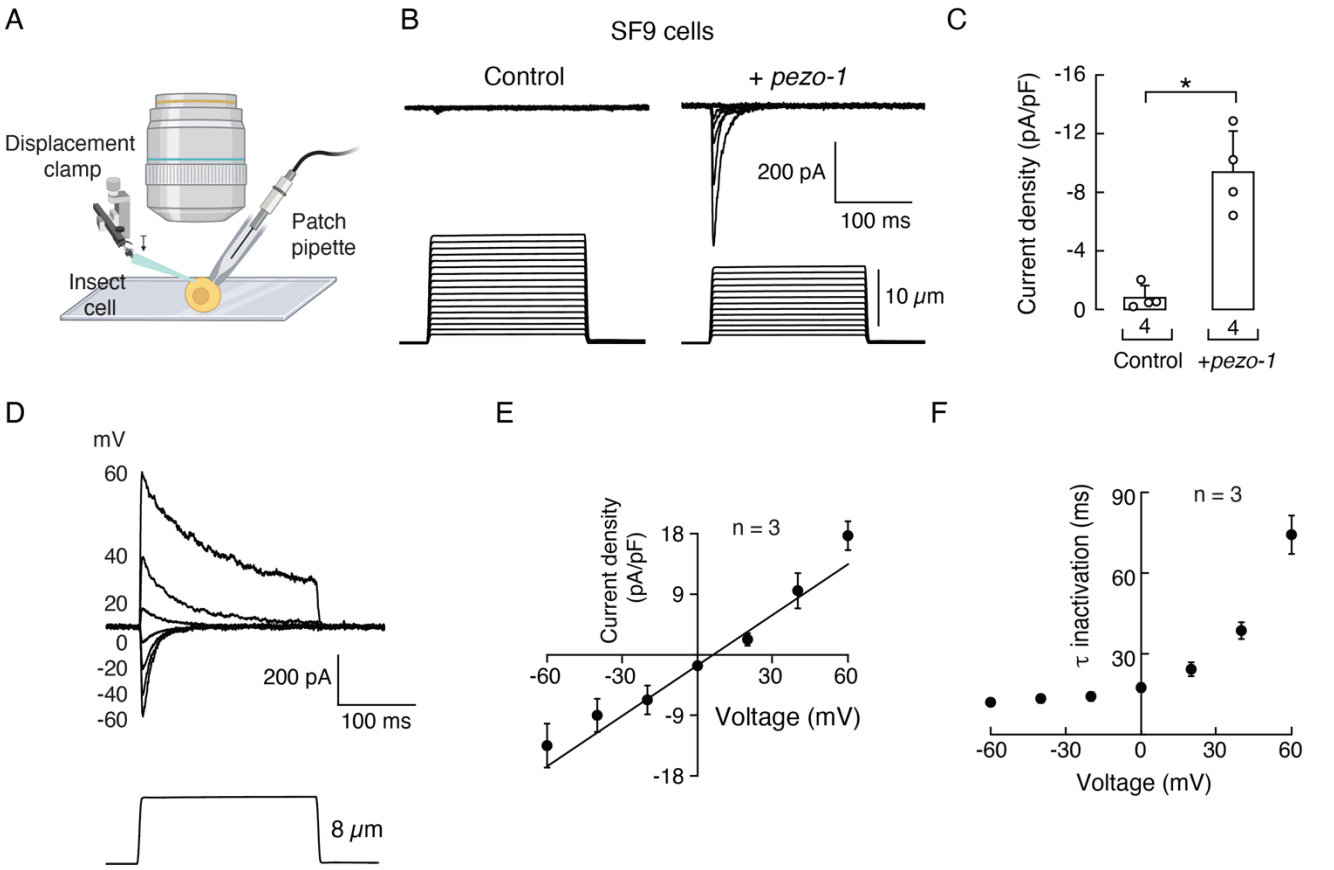

Figure 8. Sf9 cells infected with a *pezo-1*-containing baculovirus display mechanosensitive currents. (**A**) Schematic representation of the mechanical stimulation protocol applied to Sf9 cells infected with a baculovirus containing *pezo-1* recorded in the whole-cell configuration. Created with BioRender.com. (**B**) Representative whole-cell patch-clamp recordings (at −60 mV) of Sf9 cells control or infected with a baculovirus containing *pezo-1* elicited by mechanical stimulation. (**C**) Current densities of Sf9 cells control or infected with a baculovirus containing *pezo-1* elicited by maximum displacement. n is denoted above the *x*-axis. Mann–Whitney test. Asterisk indicates values significantly different (*p < 0.05). (**D**) Representative whole-cell patch-clamp recordings of Sf9 cells infected with a baculovirus containing *pezo-1* elicited by mechanical stimulation (bottom) at constant voltages ranging from -60 to +60 mV. (**E**) Current-voltage relation recorded at a constant displacement of 8 µm in the whole-cell configuration. The reversal potential is 6.74 mV. Each circle represents the mean ± SD. (**F**) PEZO-1 time constants of inactivation elicited by maximum displacement at constant voltages ranging from -60 to +60 mV. Each circle represents the mean ± SD.

DISCUSSION

In 2010, Coste and collaborators reported that the *C. elegans* genome contained a single *Piezo* gene, *pezo-1* (Coste *et al.*, 2010). However, the functional role of *pezo-1* remained elusive even after a decade of its discovery. Here, we showed that PEZO-1 is a mechanosensitive channel with a novel functional role in the worm pharynx by combining fluorescent reporters, genome editing, electropharyngeogram, behavioral, and patch-clamp measurements. We found that *pezo-1* is highly expressed in neurons involved in pharyngeal pumping relaxation. In addition to its expression, several lines of evidence suggested that PEZO-1 modulated several discrete but reliable features of the pharyngeal function. Lack- or augmentation- of PEZO-1 function increased pharyngeal pumping frequencies when worms were challenged with 2 mM serotonin, hyperosmotic conditions, or fed with control bacteria. In the absence of functional PEZO-1, worms reduced pharyngeal function (i.e., low frequency and long pump intervals) when fed with spaghetti-like bacteria. Finally, we demonstrated that the *pezo*-1 gene encodes a mechanosensitive ion channel. Altogether, our results established that PEZO-1 is important for pharyngeal function regulation and food sensation.

C. elegans feeding relies on the ability of its pharynx to contract and relax. The pharynx is a tube of electrically coupled muscle cells that continuously pump throughout the worm's life (Mango, 2007). Several ion channels have been identified to be crucial for the pharyngeal muscle action potential, including acetylcholine receptors, T- and L-type Ca^{2+} channels, glycine receptors, and K^{+} channels (Avery and You, 2012). Although the pharyngeal muscle is capable of pumping (albeit at low frequencies) without nervous system input, higher pumping frequencies are controlled by pharyngeal motor neurons, namely $MC_{L/R}$ and $M3_{L/R}$ (Avery and You, 2012). Nevertheless, the role of the nervous system in the control of rhythmic pharyngeal pumping is not completely understood. It is known, however, that the pharynx responds to a variety of neuromodulators (Avery and Horvitz, 1989). We found that *pezo-1* is expressed in proprioceptive/mechanosensory neurons $NSM_{L/R}$ and $M3_{L/R}$ (both important for the pharyngeal nervous system) and in the pharyngeal interneuron I3 (Avery and Horvitz, 1989). Unlike $NSM_{L/R}$ and $M3_{L/R}$, the function of I3 has not been established (Avery,

1993; Avery and Thomas, 1997). Our results suggest that PEZO-1 is not essential for pharyngeal muscles, but fine tunes the role of the nervous system controlling the pharynx function. This is reminiscent of the novel role of mammalian PIEZO1 and PIEZO2 mediating neuronal sensing of blood pressure and the baroreceptor reflex (Zeng *et al.*, 2018).

$NSM_{L/R}$ and $M3_{L/R}$, both *pezo-1*-expressing neurons, have been postulated to sense bacteria in the pharynx lumen via their proprioceptive endings and secrete serotonin in response to this mechanical stimulus (Avery, 1993; Avery and Thomas, 1997). Laser ablation of $NSM_{L/R}$ in *unc-29* mutants leads to subtle changes in pharyngeal pumping rate; however, this was done while simultaneously ablating other pharyngeal motor neurons (M1, $M2_{L/R}$, $M3_{L/R}$, M5, and MI) (Avery, 1993). This approach could exert antagonistic effects on pumping rate yielding a steady pharyngeal activity. Using the Screenchip^{TM} system allowed us to reveal the potential roles of extrapharyngeal neurons expressing *pezo-1* ($NSM_{L/R}$ and $M3_{L/R}$). Our results determined that activation of PEZO-1 inhibited serotonin-dependent fast pumping rate in the absence of food. They further demonstrated that PEZO-1 modulated the feeding behavior of worms confronted to various food consistencies (control and spaghetti-like bacteria). This led us to hypothesize that PEZO-1 is involved in food sensation and modulates pharyngeal pumping rate. Hence, similar to the mammalian ortholog PIEZO2, PEZO-1 is expressed in proprioceptive endings and involved in stretch reflexes (Woo *et al.*, 2015; Chesler *et al.*, 2016). Nevertheless, it remains to be determined if mammalian PIEZO channels play a role in food sensation and/or the swallowing reflex.

Humans sense various organoleptic food qualities such as visual aspects (color and shape), odorants through smell, and texture and flavor through tasting. In nematodes, there is a lack of understanding of what is sensed as food. Worms are able to filter particles from fluid in a size-dependent manner (Fang-Yen, Avery and Samuel, 2009; Kiyama, Miyahara and Ohshima, 2012) and feeding is facilitated by attractive odors or suppressed by repellents (e.g., diacetyl, isoamyl alcohol, quinine) (Gruninger, Gualberto and Garcia, 2008; Li *et al.*, 2012). Others have demonstrated that worms prefer to feed from active (i.e., bacteria reproducing rapidly and emitting high levels of CO_2)

rather than inactive bacteria (Yu *et al.*, 2015). We determined that *pezo-1* KO worms "choke" when presented with spaghetti-like bacteria, whereas WT and GOF strains increase pharyngeal pumping when ingesting this elongated food. Therefore, we propose that the pharynx itself might be a sensory organ, as worms modify their pumping parameters when they sense solutions of different osmolarities or food with different textures and/or consistencies. We further hypothesized that worms are able to perceive changes in texture and adjust their pumping frequency by a mechanism requiring PEZO-1. Since *pezo-1* is not essential for *C. elegans* when cultured in standard laboratory conditions (e.g., monoaxenically on *E. coli* OP50), we wonder if in its natural biotic environment this mechanosensitive ion channel plays a crucial role, as it does in humans and *Drosophila*. Given that worms grow in microbe-rich and heterogenous environments (feeding from prokaryotes of the genera *Acetobacter*, *Gluconobacter*, and *Enterobacter*) (Schulenburg and Félix, 2017), they might encounter bacteria of different dimensions and textures that will make *pezo-1* function more relevant to the worm's ability to discriminate the food on which it grows best.

Why *pezo-1* loss- and gain-of-function mutations cause similar behavior phenotypes? Our data show that both *pezo-1* mutants (KO and GOF) increase the pumping frequency of the pharynx in different settings: serotonin exposure, high osmolarity, and ingestion of control bacteria. While it may seem counterintuitive at first, there are several scenarios in which too little or too much mechanosensation can be detrimental for animal's behaviors. For instance, the *mec-4* gene encodes for the DEG/ENaC ion channel subunit of the mechanoelectrical transduction channel complex in touch. Like our *pezo-1* mutants that lack control of pharyngeal pumping function, LOF (*u253*, a deletion) and GOF (*e1611*, missense mutation A713V) alleles of the *mec-4* gene render touch-insensitive worms (Driscoll and Chalfie, 1991; Hong, Mano and Driscoll, 2000; O'Hagan, Chalfie and Goodman, 2005). Similarly, *deg-1*, a DEG/ENaC ion channel subunit expressed in ASH neurons, LOF (*u443*, eliminates the 3' end of *deg-1*) and GOF (*u506*, missense mutation A393T) alleles decrease the worm's ability to respond to nose touch (Savage *et al.*, 1989; García-Añoveros, Ma and Chalfie, 1995; Geffeney *et al.*, 2011). In humans, *PIEZO2* LOF (premature stop codon) and GOF (missense mutation

I802F) alleles caused joint contractures, skeletal abnormalities and alterations in muscle tone (Coste *et al.*, 2013; Chesler *et al.*, 2016; Yamaguchi *et al.*, 2019). Only when feeding worms, the spaghetti-like bacteria, we were able to uncover a difference between the LOF and the GOF mutants. Hence, we hypothesize that lacking the function of PEZO-1 significantly slows down pharyngeal function when passing down the lengthy bacteria from the pharynx to the gut.

Several requirements must be met for a channel to be considered mechanically gated (Arnadóttir and Chalfie, 2010). Accordingly, we found that *pezo-1* is expressed in the proprioceptive neuron NSM, knocking out *pezo-1* inhibits worm's pharyngeal function when challenged with hyperosmolarity or elongated bacteria, engineering a single point mutation in the putative pore domain (R2373K) elicited similar activation and deactivation delays that are reminiscent of the gating behavior reported for the human PIEZO1 R2456K (Bae *et al.*, 2013), and expression of *pezo-1* confers mechanosensitivity to, otherwise naïve, Sf9 cells. We propose that PEZO-1 is a mechanosensitive ion channel directly gated by bilayer tension given that the time it takes to reach half of the steady state currents ranges between 3.5 to 15 ms upon application of negative pressure. These are faster than activation times reported for the *Drosophila* phototransduction cascade, one of the quickest second messenger cascades (Hardie, 2001). These combined efforts highlight the versatile functions of the PIEZO mechanosensitive channel family as well as the strength of the model organism *C. elegans* to reveal physiological functions.

Our findings revealing PEZO-1 as a mechanosensitive ion channel that modulates pharyngeal function raise several important questions. How does *pezo-1* modulate pumping behavior electrical activity? Does *pezo-1* equally enhance or inhibit the function of the pharyngeal hypodermal, gland and muscle cells, and neurons expressing this channel? Could *pezo-1* phenotypes be exacerbated if the gene function is nulled in a cell-specific manner? Does PEZO-1 require auxiliary subunits and/or cytoskeleton for gating? Regardless of the answers, the plethora of physiological roles that this eukaryotic family of mechanosensitive ion channels play is outstanding. More experimental insight will be needed to grasp the full implications of *pezo*-1 in the physiology of *C. elegans*.

Acknowledgements

The authors thank Dr. Julio F. Cordero-Morales, Dr. Andrés G. Vidal-Gadea, and Dr. Christopher E. Hopkins for critically reading the manuscript, and Dr. Rebeca Caires, MSc Briar Bell, and MBBS Soumi Mazumdar for technical assistance. *C. elegans* (N2, DA572, and DA1051) and *E. coli* strains (OP50 and NA22) were obtained from the *Caenorhabditis* Genetics Center, which is funded by the NIH Office of Research Infrastructure Programs (P40 OD010440). LX960 was provided by Dr. Kevin Collins (University of Miami). This work was supported by the American Heart Association (16SDG26700010 to VV) and the National Institutes of Health (R01GM133845 to VV) and the Neuroscience Institute at UTHSC (Research Associate Matching Salary Support to JL).

Competing interests

The authors declare no competing financial interests.

Author contributions

Conceptualization, VV; Methodology, VV and JRMM; Investigation, JRMM, LOR, and JL; Writing, VV and JRMM; Funding Acquisition, VV; Supervision, VV.

.

Comparison	p-*value*
'0mM' *vs* '2mM'	2.31E-31
'0mM' *vs* '5mM'	8.82E-40
'0mM' *vs* '10mM'	1.88E-40
'0mM' *vs* '20mM'	1.88E-40
'2mM' *vs* '5mM'	3.52E-16
'2mM' *vs* '10mM'	7.35E-25
'2mM' *vs* '20mM'	9.25E-28
'5mM' *vs* '10mM'	0.000142
'5mM' *vs* '20mM'	1.77E-06
'10mM' *vs* '20mM'	0.10003

Table I. Statistical comparison of serotonin concentration probability densities by Kolmogorov-Smirnov (Figure 2c).

REFERENCES

Albertson, D. G. and Thomson, J. N. (1976) "The pharynx of Caenorhabditis elegans," *Philosophical Transactions of the Royal Society of London. B, Biological Sciences*, 275(938), pp. 299–325. doi: 10.1098/rstb.1976.0085.

Albuisson, J. *et al.* (2013) "Dehydrated hereditary stomatocytosis linked to gain-of-function mutations in mechanically activated PIEZO1 ion channels," *Nature Communications*, 4(May). doi: 10.1038/ncomms2899.

Alper, S. L. (2017) "Genetic Diseases of PIEZO1 and PIEZO2 Dysfunction," *Current Topics in Membranes*, 79. doi: 10.1016/bs.ctm.2017.01.001.

ben Arous, J., Laffont, S. and Chatenay, D. (2009) "Molecular and Sensory Basis of a Food Related Two-State Behavior in C. elegans," *PLoS ONE*. Edited by V. Brezina, 4(10), p. e7584. doi: 10.1371/journal.pone.0007584.

Arnadóttir, J. and Chalfie, M. (2010). "Eukaryotic mechanosensitive channels. *Annu Rev Biophys.*, pp. 39:111-37. doi: 10.1146/annurev.biophys.37.032807.125836. PMID: 20192782.

Avery, L. (1993) "Motor neuron M3 controls pharyngeal muscle relaxation timing in Caenorhabditis elegans.," *The Journal of experimental biology*, 175, pp. 283–297.

Avery, L., Bargmann, C. I. and Horvitz, H. R. (1993) "The Caenorhabditis elegans unc-31 gene affects multiple nervous system-controlled functions.," *Genetics*, 134(2), pp. 455–64. Available at: http://www.ncbi.nlm.nih.gov/pubmed/8325482.

Avery, L. and Horvitz, H. R. (1989) "Pharyngeal pumping continues after laser killing of the pharyngeal nervous system of C. elegans," *Neuron*, 3(4), pp. 473–485. doi: 10.1016/0896-6273(89)90206-7.

Avery, L. and Thomas, J. H. (1997) "Feeding and Defecation," in. Cold Spring Harbor Laboratory Press, Cold Spring Harbor (NY). Available at: https://www.ncbi.nlm.nih.gov/books/NBK20138.

Avery, L. and You, Y.-J. (2012) "C. elegans feeding.," *WormBook : the online review of C. elegans biology*, pp. 1–23. doi: 10.1895/wormbook.1.150.1.

Bae, C. *et al.* (2013) "Xerocytosis is caused by mutations that alter the kinetics of the mechanosensitive channel PIEZO1," *Proceedings of the National Academy of Sciences of the United States of America*, 110(12). doi: 10.1073/pnas.1219777110.

Bai, X. *et al.* (2020) "Caenorhabditis elegans piezo channel coordinates multiple reproductive tissues to govern ovulation," *eLife*, 9, pp. 1–35. doi: 10.7554/eLife.53603.

Chesler, A. T. *et al.* (2016) "The Role of PIEZO2 in Human Mechanosensation.," *The New England journal of medicine*, 375(14), pp. 1355–1364. doi: 10.1056/NEJMoa1602812.

Coste, B. *et al.* (2010) "Piezo1 and Piezo2 Are Essential Components of Distinct Mechanically Activated Cation Channels," *Science*, 330(6000), pp. 55–60. doi: 10.1126/science.1193270.

Coste, B. *et al.* (2012). "Piezo proteins are pore-forming subunits of mechanically activated channels". *Nature*, 483(7388), pp. 176-81. doi: 10.1038/nature10812.

Coste, B. *et al.* (2013) "Gain-of-function mutations in the mechanically activated ion channel PIEZO2 cause a subtype of Distal Arthrogryposis," *Proceedings of the National Academy of Sciences of the United States of America*, 110(12). doi: 10.1073/pnas.1221400110.

Cox, C. D., Bavi, N. and Martinac, B. (2019) "Biophysical Principles of Ion-Channel-Mediated Mechanosensory Transduction," *Cell Reports*. doi: 10.1016/j.celrep.2019.08.075.

Dent, J. A., Davis, M. W. and Avery, L. (1997) "avr-15 encodes a chloride channel subunit that mediates inhibitory glutamatergic neurotransmission and ivermectin sensitivity in Caenorhabditis elegans," *The EMBO Journal*, 16(19), pp. 5867–5879. doi: 10.1093/emboj/16.19.5867.

Douguet, D. and Honoré, E. (2019) "Mammalian Mechanoelectrical Transduction: Structure and Function of Force-Gated Ion Channels.," *Cell*, 179(2), pp. 340–354. doi: 10.1016/j.cell.2019.08.049.

Driscoll, M. and Chalfie, M. (1991) "The mec-4 gene is a member of a family of Caenorhabditis elegans genes that can mutate to induce neuronal degeneration," *Nature*, 349(6310), pp. 588–593. doi: 10.1038/349588a0.

613 Fang-Yen, C., Avery, L. and Samuel, A. D. T. (2009) "Two size-selective mechanisms specifically
614 trap bacteria-sized food particles in Caenorhabditis elegans," *Proceedings of the National Academy*
615 *of Sciences*, 106(47), pp. 20093–20096. doi: 10.1073/pnas.0904036106.
616 García-Añoveros, J., Ma, C. and Chalfie, M. (1995) "Regulation of Caenorhabditis elegans
617 degenerin proteins by a putative extracellular domain," *Current Biology*, 5(4), pp. 441–448. doi:
618 10.1016/S0960-9822(95)00085-6.
619 Geffeney, S. L. *et al.* (2011) "DEG/ENaC but not TRP channels are the major mechanoelectrical
620 transduction channels in a c. Elegans nociceptor," *Neuron*, 71(5), pp. 845–857. doi:
621 10.1016/j.neuron.2011.06.038.
622 Geffeney, S. L. and Goodman, M. B. (2012) "How we feel: ion channel partnerships that detect
623 mechanical inputs and give rise to touch and pain perception.," *Neuron*, 74(4), pp. 609–19. doi:
624 10.1016/j.neuron.2012.04.023.
625 Gruninger, T. R., Gualberto, D. G. and Garcia, L. R. (2008) "Sensory perception of food and insulin-
626 like signals influence seizure susceptibility.," *PLoS genetics*, 4(7), p. e1000117. doi:
627 10.1371/journal.pgen.1000117.
628 Hamilton, E. S., Schlegel, A. M. and Haswell, E. S. (2015) "United in diversity: mechanosensitive
629 ion channels in plants.," *Annual review of plant biology*, 66, pp. 113–37. doi: 10.1146/annurev-
630 arplant-043014-114700.
631 Hardie, R. C. (2001) "Phototransduction in Drosophila melanogaster," *Journal of Experimental*
632 *Biology*.
633 Hasse, S., Hyman, A. A. and Sarov, M. (2016) "TransgeneOmics – A transgenic platform for protein
634 localization based function exploration," *Methods*, 96, pp. 69–74. doi: 10.1016/j.ymeth.2015.10.005.
635 Höflich, J. *et al.* (2004) "Loss of srf-3 -encoded Nucleotide Sugar Transporter Activity in C
636 aenorhabditis elegans Alters Surface Antigenicity and Prevents Bacterial Adherence," *Journal of*
637 *Biological Chemistry*, 279(29), pp. 30440–30448. doi: 10.1074/jbc.M402429200.
638 Hong, K., Mano, I. and Driscoll, M. (2000) "In vivo structure-function analyses of Caenorhabditis
639 elegans MEC-4, a candidate mechanosensory ion channel subunit," *Journal of Neuroscience*, 20(7),
640 pp. 2575–2588. doi: 10.1523/jneurosci.20-07-02575.2000.
641 Ikeda, R. *et al.* (2014) "Merkel cells transduce and encode tactile stimuli to drive Aβ-afferent
642 impulses.," *Cell*, 157(3), pp. 664–75. doi: 10.1016/j.cell.2014.02.026.
643 Keane, J. and Avery, L. (2003) "Mechanosensory inputs influence Caenorhabditis elegans
644 pharyngeal activity via ivermectin sensitivity genes.," *Genetics*, 164(1), pp. 153–62. Available at:
645 http://www.ncbi.nlm.nih.gov/pubmed/12750328.
646 Kim, S. E. *et al.* (2012) "The role of Drosophila Piezo in mechanical nociception," *Nature*,
647 483(7388). doi: 10.1038/nature10801.
648 Kiyama, Y., Miyahara, K. and Ohshima, Y. (2012) "Active uptake of artificial particles in the
649 nematode Caenorhabditis elegans," *Journal of Experimental Biology*, 215(7), pp. 1178–1183. doi:
650 10.1242/jeb.067199.
651 Kung, C., Martinac, B. and Sukharev, S. (2010) "Mechanosensitive channels in microbes.," *Annual*
652 *review of microbiology*, 64, pp. 313–29. doi: 10.1146/annurev.micro.112408.134106.
653 Lee, K. S. *et al.* (2017) "Serotonin-dependent kinetics of feeding bursts underlie a graded response to
654 food availability in C. elegans," *Nature Communications*, 8(1), p. 14221. doi:
655 10.1038/ncomms14221.
656 Lee, R. Y. N. *et al.* (1999) "EAT-4, a Homolog of a Mammalian Sodium-Dependent Inorganic
657 Phosphate Cotransporter, Is Necessary for Glutamatergic Neurotransmission in Caenorhabditis
658 elegans," *The Journal of Neuroscience*, 19(1), pp. 159–167. doi: 10.1523/JNEUROSCI.19-01-
659 00159.1999.
660 Li, J. *et al.* (2014) "Piezo1 integration of vascular architecture with physiological force," *Nature*,
661 515(7526). doi: 10.1038/nature13701.
662 Li, Z. *et al.* (2012) "Dissecting a central flip-flop circuit that integrates contradictory sensory cues in
663 C. elegans feeding regulation," *Nature Communications*, 3(1), p. 776. doi: 10.1038/ncomms1780.
664 Ma, S. *et al.* (2018) "Common PIEZO1 Allele in African Populations Causes RBC Dehydration and
665 Attenuates Plasmodium Infection," *Cell*, 173(2). doi: 10.1016/j.cell.2018.02.047.

Maksimovic, S. *et al.* (2014) "Epidermal Merkel cells are mechanosensory cells that tune mammalian touch receptors.," *Nature*, 509(7502), pp. 617–21. doi: 10.1038/nature13250.
Mango, S. E. (2007) "The C. elegans pharynx: a model for organogenesis.," *WormBook : the online review of C. elegans biology*, pp. 1–26. doi: 10.1895/wormbook.1.129.1.
Martinac, B. *et al.* (1987) "Pressure-sensitive ion channel in Escherichia coli," *Proceedings of the National Academy of Sciences of the United States of America*, 84(8), pp. 2297–2301. doi: 10.1073/pnas.84.8.2297.
Min, S. *et al.* (2020) "Control of feeding by Piezo-mediated gut mechanosensation in Drosophila 1 2," *bioRxiv*, p. 2020.09.11.293712. Available at: https://doi.org/10.1101/2020.09.11.293712.
Murthy, S. E. *et al.* (2018) "The mechanosensitive ion channel Piezo2 mediates sensitivity to mechanical pain in mice," *Science Translational Medicine*, 10(462), p. eaat9897. doi: 10.1126/scitranslmed.aat9897.
Niacaris, T. (2003) "Serotonin regulates repolarization of the C. elegans pharyngeal muscle," *Journal of Experimental Biology*, 206(2), pp. 223–231. doi: 10.1242/jeb.00101.
O'Hagan, R., Chalfie, M. and Goodman, M. B. (2005) "The MEC-4 DEG/ENaC channel of Caenorhabditis elegans touch receptor neurons transduces mechanical signals.," *Nature neuroscience*, 8(1), pp. 43–50. doi: 10.1038/nn1362.
Ohmachi, M. *et al.* (1999) "kel-1, a novel Kelch-related gene in Caenorhabditis elegans, is expressed in pharyngeal gland cells and is required for the feeding process," *Genes to Cells*, 4(6), pp. 325–337. doi: 10.1046/j.1365-2443.1999.00264.x.
Pan, B. *et al.* (2018) "TMC1 Forms the Pore of Mechanosensory Transduction Channels in Vertebrate Inner Ear Hair Cells.," *Neuron*, 99(4), pp. 736-753.e6. doi: 10.1016/j.neuron.2018.07.033.
Parpaite, T. and Coste, B. (2017) "Piezo channels," *Current Biology*, 27(7), pp. R250–R252. doi: 10.1016/j.cub.2017.01.048.
Pathak, M. M. *et al.* (2014) "Stretch-activated ion channel Piezo1 directs lineage choice in human neural stem cells.," *Proceedings of the National Academy of Sciences of the United States of America*, 111(45), pp. 16148–53. doi: 10.1073/pnas.1409802111.
Raizen, D. M. and Avery, L. (1994) "Electrical activity and behavior in the pharynx of caenorhabditis elegans," *Neuron*, 12(3), pp. 483–495. doi: 10.1016/0896-6273(94)90207-0.
Raizen, D. M., Lee, R. Y. N. and Avery, L. (1995) "Interacting genes required for pharyngeal excitation by motor neuron MC in Caenorhabditis elegans," *Genetics*, 141(4), pp. 1365–1382.
Ranade, S. S. *et al.* (2014) "Piezo2 is the major transducer of mechanical forces for touch sensation in mice.," *Nature*, 516(7529), pp. 121–5. doi: 10.1038/nature13980.
Retailleau, K. *et al.* (2015) "Piezo1 in Smooth Muscle Cells Is Involved in Hypertension-Dependent Arterial Remodeling.," *Cell reports*, 13(6), pp. 1161–1171. doi: 10.1016/j.celrep.2015.09.072.
Rode, B. *et al.* (2017) "Piezo1 channels sense whole body physical activity to reset cardiovascular homeostasis and enhance performance.," *Nature communications*, 8(1), p. 350. doi: 10.1038/s41467-017-00429-3.
Romero, L. O. *et al.* (2019) "Dietary fatty acids fine-tune Piezo1 mechanical response," *Nature Communications*, 10(1), pp. 1–14. doi: 10.1038/s41467-019-09055-7.
Savage, C. *et al.* (1989) "mec-7 is a beta-tubulin gene required for the production of 15-protofilament microtubules in Caenorhabditis elegans.," *Genes & development*, 3(6), pp. 870–881. doi: 10.1101/gad.3.6.870.
Schindelin, J. *et al.* (2009) "Fiji - an Open platform for biological image analysis," *Nature Methods*, 9(7). doi: 10.1038/nmeth.2019.Fiji.
Schulenburg, H. and Félix, M. A. (2017) "The natural biotic environment of Caenorhabditis elegans," *Genetics*, 206(1), pp. 55–86. doi: 10.1534/genetics.116.195511.
Shtonda, B. B. and Avery, L. (2006) "Dietary choice behavior in Caenorhabditis elegans," *Journal of Experimental Biology*, 209(1), pp. 89–102. doi: 10.1242/jeb.01955.
Singh, R. N. and Sulston, J. E. (1978) "Some Observations On Moulting in Caenorhabditis Elegans," *Nematologica*, 24(1), pp. 63–71. doi: 10.1163/187529278X00074.

718 Smit, R. B., Schnabel, R. and Gaudet, J. (2008) "The HLH-6 Transcription Factor Regulates C.
719 elegans Pharyngeal Gland Development and Function," *PLoS Genetics*. Edited by S. E. Mango,
720 4(10), p. e1000222. doi: 10.1371/journal.pgen.1000222.
721 Strange, K., Christensen, M. and Morrison, R. (2007) "Primary culture of Caenorhabditis elegans
722 developing embryo cells for electrophysiological, cell biological and molecular studies," *Nature*
723 *Protocols*, 2(4), pp. 1003–1012. doi: 10.1038/nprot.2007.143.
724 Szczot, M. *et al.* (2018) "PIEZO2 mediates injury-induced tactile pain in mice and humans," *Science*
725 *Translational Medicine*, 10(462), p. eaat9892. doi: 10.1126/scitranslmed.aat9892.
726 Taylor, S. R. *et al.* (2020) "Molecular topography of an entire nervous system," *bioRxiv*. doi:
727 10.1101/2020.12.15.422897.
728 Trojanowski, N. F., Raizen, D. M. and Fang-Yen, C. (2016) "Pharyngeal pumping in Caenorhabditis
729 elegans depends on tonic and phasic signaling from the nervous system," *Scientific Reports*, 6(1), p.
730 22940. doi: 10.1038/srep22940.
731 Tsujimura, T. *et al.* (2019) "Involvement of the epithelial sodium channel in initiation of
732 mechanically evoked swallows in anaesthetized rats," *Journal of Physiology*, 597(11). doi:
733 10.1113/JP277895.
734 Vidal-Gadea, A. G. *et al.* (2012) " Coordination of behavioral hierarchies during environmental
735 transitions in Caenorhabditis elegans ," *Worm*, 1(1), pp. 5–11. doi: 10.4161/worm.19148.
736 Wang, P. *et al.* (2020) "Visceral Mechano-sensing Neurons Control Drosophila Feeding by Using
737 Piezo as a Sensor," *Neuron*, pp. 1–11. doi: 10.1016/j.neuron.2020.08.017.
738 Wang, S. *et al.* (2016) "Endothelial cation channel PIEZO1 controls blood pressure by mediating
739 flow-induced ATP release," *Journal of Clinical Investigation*, 126(12), pp. 4527–4536. doi:
740 10.1172/JCI87343.
741 Woo, S.-H. *et al.* (2014) "Piezo2 is required for Merkel-cell mechanotransduction.," *Nature*,
742 509(7502), pp. 622–6. doi: 10.1038/nature13251.
743 Woo, S.-H. *et al.* (2015) "Piezo2 is the principal mechanotransduction channel for proprioception,"
744 *Nature Neuroscience*, 18(12), pp. 1756–1762. doi: 10.1038/nn.4162.
745 Wu, J., Lewis, A. H. and Grandl, J. (2017) "Touch, Tension , and Transduction – The Function and
746 Regulation of Piezo Ion Channels," *Trends in Biochemical Sciences*, 42(1), pp. 57–71. doi:
747 10.1016/j.tibs.2016.09.004.
748 Wu, J. *et al.* (2017) "Inactivation of Mechanically Activated Piezo1 Ion Channels Is Determined by
749 the C-Terminal Extracellular Domain and the Inner Pore Helix". *Cell Report*s. 21(9) pp. 2357-2366.
750 doi: 10.1016/j.celrep.2017.10.120.
751 Yamaguchi, T. *et al.* (2019) "PIEZO2 deficiency is a recognizable arthrogryposis syndrome: A new
752 case and literature review," *American Journal of Medical Genetics, Part A*, 179(6). doi:
753 10.1002/ajmg.a.61142.
754 Yan, Z. *et al.* (2013) "Drosophila NOMPC is a mechanotransduction channel subunit for gentle-
755 touch sensation.," *Nature*, 493(7431), pp. 221–5. doi: 10.1038/nature11685.
756 Yu, L. *et al.* (2015) "Bacterial respiration and growth rates affect the feeding preferences, brood size
757 and lifespan of Caenorhabditis elegans," *PLoS ONE*, 10(7), pp. 1–13. doi:
758 10.1371/journal.pone.0134401.
759 Zarychanski, R. *et al.* (2012) "Mutations in the mechanotransduction protein PIEZO1 are associated
760 with hereditary xerocytosis," *Blood*, 120(9), pp. 1908–1915. doi: 10.1182/blood-2012-04-422253.
761 Zeng, W.-Z. *et al.* (2018) "PIEZOs mediate neuronal sensing of blood pressure and the baroreceptor
762 reflex.," *Science (New York, N.Y.)*, 362(6413), pp. 464–467. doi: 10.1126/science.aau6324.

763